# EDITORIAL BOARD

## EDITOR-IN-CHIEF

R. Ahmad, Centre for Advanced Studies in Physics,
Government College University, Lahore-54000, PAKISTAN
E-mail: jnsm@gcu.edu.pk
http://www.gcu.edu.pk/FullTextJour/JNSM_Phy/JNSM.htm

| | |
|---|---|
| M. Akram | (Editor) |
| A. Shahbaz | (Editor) |
| A. U. Khan | (Associate Editor) |

## ADVISORY BOARD

| Panel of Foreign Advisors | Panel of Local Advisors |
|---|---|
| **J. Meng**<br>P. R. China | **M. Zakaullah**<br>QAU, Islamabad |
| **K. P. Shum**<br>Hong Kong University, China (SAR) | **M. A. Malik**<br>Hamdard Institute of Information Technology, Islamabad |
| **N. Tsintsadze**<br>Institute of Physics, Tbitsi, Georgia | **M. S. Iqbal**<br>F. C. College, Lahore |
| **Salimullah**<br>Dhaka University, Bangladesh | **H. A. Shah**<br>GC University, Lahore |
| **T. Kaladze**<br>Tblisi State University, Georgia | **N. A. D. Khattak**<br>Gomal University, D.I. Khan |
| **J. S. Pan**<br>IMRE Singapore | **K. Ahmad**<br>School of Computer Sciences, NCBA&E, Lahore |
| **P. Lee**<br>NTU Singapore | **E. Sandhu**<br>School of Computer Sciences, NCBA&E, Lahore |
| **R. S. Rawat**<br>NTU Singapore | **A. M. Mirza**<br>QAU, Islamabad |
| | **K. H. Dar**<br>Leeds University, Lahore |



**Annual Subscription**

Pakistan: Rs 250    Foreign Countries: US$ 40    Overseas Air Mail Charges: US$ 10

**The Journal is published bi-annually**
**In April and October**

**Published by:**
Riaz Ahmad for Government College University, Lahore, Pakistan

**Printed at:**
Mithas Enterprises Press, Lahore

# CONTENTS


| Sr. No. | TITLE | PAGE |
|---|---|---|
| 1. | CHARACTERIZATION AND EFFECT OF ARGON-NITROGEN PLASMA ON NITRIDATION OF ALUMINUM ALLOY<br>M. S. SHAH, N. KHAN AND R. AHMAD | 01 |
| 2. | JORDAN ZERO-PRODUCT PRESERVING ADDITIVE MAPS ON NEST ALGEBRAS<br>A. MAJEED AND J. Li | 19 |
| 3. | INVESTIGATION BY SYNCHROTRON RADIATION OF InGaAs LASING STRUCTURES GROWN ON SiGe/Si PSEUDOSUBSTRATES<br>A. R. KHAN, K. MUNDBOTH, J. STANGL, M. MEDUŇA, E. WINTERSBERGER AND G. BAUER | 27 |
| 4. | COMMON FIXED POINT THEOREMS IN FUZZY METRIC SPACES FOR SEMI-COMPATIBLE MAPPINGS<br>M. A. KHAN, SUMITRA AND R. CHUGH | 33 |
| 5. | PREPARATION AND CHARACTERIZATION OF $SrBi_2Ta_2O_9$ (SBT) THIN FILMS<br>Z. N. KAYANI, S. RIAZ AND S. NASEEM | 49 |

# JOURNAL OF NATURAL SCIENCES AND MATHEMATICS
## INFORMATION FOR AUTHORS

### 1. TYPES OF PAPERS ACCEPTED

The Journal aims at publishing original research papers and the review papers from distinguished scientists on Mathematics, Physics, Chemistry and Computer Science.

### 2. SUBMISSION OF MANUSCRIPTS

Manuscripts should be submitted in duplicate to the Section Editor concerned. All papers are refereed. The decision of the Editorial Board regarding the acceptance and publication of the paper will be final.

### 3. PREPARATION OF MANUSCRIPT

#### 3.1 Language and Style

All submissions should be in English, typed in double spacing on one side of the paper only with a left hand margin of at least 4 cm. Mathematical expressions must be carefully printed. Computer composed manuscript on C.D. in Microsoft Word is required for speedy publication.

#### 3.2 Abstract

This should comprise a brief and factual summary of contents and should be suitable for direct use by abstracting journals. This will seldom require more than 200 words.

#### 3.3 Section/Sub-Section Headings

Papers should be divided into sections / sub-sections and numbered as exemplified in the headings of this INFORMATION FOR AUTHORS.

#### 3.4 References

References should be numbered consecutively in the text, e.g. "According to a recent theory [6]…it is well established [7]" and collected at the end of the paper in following style:

6. I. M. Ghauri and P. Feltham, J. Nat. Sci. Math., 26 (1986) 63.
7. W. Greiner and J. Maruhn, Nuclear Models, Springer-Verlag, Berlin, (1996).

#### 3.5 Illustrations

Line diagrams must be drawn in black ink on white paper; original and two copies are required. Photographs or half-tone reproduction should be in the form of highly glazed prints. A separate list of captions for illustrations should be provided.

### 4. PROOFs

Only one set of proof is sent to the authors for correction.

PK ISSN 0022- 2941; CODEN JNSMAC
Vol. 49, No.1 & 2 (April & October 2009) PP 1-17

# CHARACTERIZATION AND EFFECT OF ARGON-NITROGEN PLASMA ON NITRIDATION OF ALUMINUM ALLOY

**M. S. SHAH, N. KHAN AND R. AHMAD**

Department of Physics, Government College University, 54000 Lahore, Pakistan
E-mail Addresses: ms_shah_sgd@yahoo.com

(Received: February 10, 2011)

**ABSTRACT:** Langmuir probe is used to determine the plasma parameters for the mixture of nitrogen-argon gases using ac generated plasma source. Results reveal that argon mixing in nitrogen plasma is an effective mode to increase electron density. Samples are exposed for 3, 6, 9 and 12 h for constant pressure (2 mbar) and electrical input power (100 W). Nitriding of aluminum alloy is performed in a mixture of argon and nitrogen plasma (1:1) plasmas, to investigate the effect of argon mixing on its surface properties. The analysis is carried out by using x-ray diffractometer (XRD), scanning electron microscopy (SEM) and Vickers micro hardness tester to investigate surface properties of the treated samples. XRD results exhibit the formation of cubic AlN thin surface layer by reactive ac sputtering with argon as a sputtering gas and nitrogen as a reactive gas. Moreover, significant increase in surface hardness is found when the sample is treated for 12 h.

**Keywords:** 50 Hz ac discharge, Plasma characterization, Nitriding, X-ray diffraction.

## 1. INTRODUCTION

Aluminum and its alloys have extensive industrial applications due to their light weight, high strength to weight ratio, good corrosion resistance and formability along with good electrical and thermal conductivities [1,2]. Aluminum nitrides are also widely investigated as an electronic and optoelectronic material as well as its favorable thermal, acoustic, optical and electrical properties. However, low surface hardness and wear resistance limit their applications in automotive, aero space and electronic industry. These surface properties can be improved by nitriding the aluminum and aluminum alloy. It is very difficult to form AlN by conventional techniques due to the formation of protective pre-existed oxide layer on the surface of aluminum alloy. The thin oxide layer prevents

**the diffusion of nitrogen into the aluminum matrix. In plasma nitriding, this oxide layer can be removed by transfer of sufficient energy during the bombardment of energetic particles [3]. The subsequent transfer of nitrogen from surface to interior of the material to form a nitrided layer is normally governed by diffusion. However, oxide layer can also be removed more effectively by sputtering prior or during nitriding with argon plasma bombardment. For this purpose argon is used to sputter the oxide layer [4,5], clean the surface and facilitate the diffusion of nitrogen into the aluminum matrix [6]. Plasma nitriding is widely used to enhance the mechanical and chemical properties of materials [7-11]. It is primarily used to enhance fatigue strength, surface hardness, wear and corrosion resistance without affecting bulk properties of materials [12,13]. Low temperature (<$500^{o}$ C) plasma nitriding is highly desirable [14], for nitrogen enriched diffusion layer with significant depth and high hardness while at higher temperatures, the deposited surface layers often show poor adhesion to the substrate [4]. The growth of nitrided surface layer follows the diffusion law and increase in layer thickness is attributed with increasing treatment time [15].**

**Another consideration in plasma processing is the production of active species and these are determined by the electron energy. Several techniques have been proposed to alter electron temperature and density [16-18]. It is found that the mixing of inert gas (Ar) in nitrogen plasma is an effective way to change the plasma parameters such as electron temperature and electron density [5]. Electron energy distribution function (EEDF), electron temperature and electron number density are important plasma parameters which influence the production of active species by inelastic collisions, plasma reactions and plasma surface interactions. Therefore, Langmuir probe [19,20] is employed for obtaining information regarding plasma parameters.**

**This paper reports the 50 Hz ac generated glow discharges which are economically attractive in industry due to their simplicity and cost-effectiveness. The present study concentrates on the effects of argon on**

**plasma parameters regarding EEDF, electron temperature, electron density and consequently on nitriding behavior of aluminum alloy with influence of processing time. This work also focused on the improvement of mechanical properties by investigating the dependence of structural and compositional properties including crystallographic structure, surface morphology and surface hardness of samples treated for different times. The influence of surface layer composition on the residual stress, hardness and tribological properties are also examined.**

## 2. EXPERIMENTAL PROCEDURES

**Aluminum alloy ($AlMg_2Si$) specimen of dimension 9×9×3 $mm^3$ are polished using SiC abrasive paper from coarse to fine grade (220 ~ 1000) on Stuers Knuth-Rotor-3 polishing machine and then cleaned ultrasonically. Nitriding of aluminum alloy is performed in cold plasma device shown in Fig. 1. It consists of a stainless steel vacuum chamber having diameter and height of 32 cm. Two circular stainless steel electrodes having 14 cm diameter and thickness of 2 cm each are adjusted in chamber in a capacitive configuration of spacing 3 cm.**

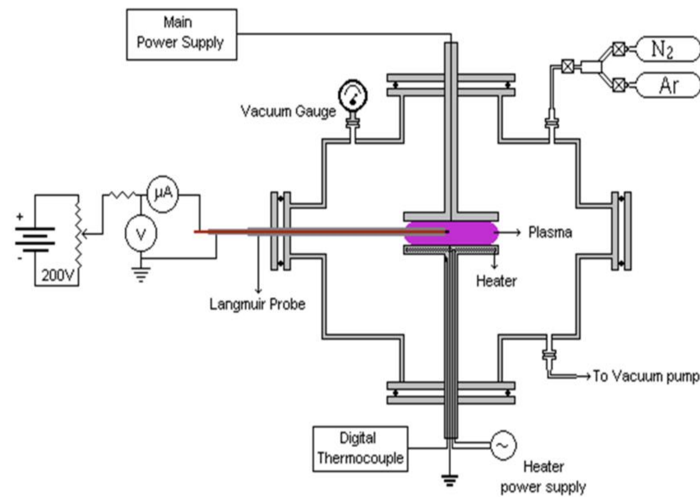


**Fig. 1: Experimental setup of the plasma nitridation system.**

The chamber is evacuated down to a pressure of $1\times10^{-2}$ mbar using a rotary vane pump. The working pressure of nitrogen and nitrogen-argon plasma is 2 mbar during nitridation process. The pressure of the chamber is measured using capsule type vacuum gauge. A 100 W ac power output from a variac transformer is applied to the top electrode through an inductive load which limits the currents during the discharge. The samples are placed on the bottom electrode which is grounded. The inlet and outlet valves are adjusted so as to maintain the desired pressure in the chamber. Langmuir probe is used as plasma diagnostic due to its easy and simple execution compared to other plasma diagnostics. Probe current is measured for DC bias voltages swept from -100 V to +100 V. For probe measurements, I-V characteristics are recorded by varying pressure from 2 mbar to 5 mbar by keeping power constant of 100 W.

Four samples are subjected to nitrogen plasma at 2-mbar pressure for 3, 6, 9, and 12 h time durations. A second set of four samples is also exposed to nitrogen-argon mixture plasma with same plasma processing parameters. During nitriding process, the temperature of the samples is maintained at $250^{o}$C by using thermocouple. After nitriding, the samples are cooled down in the chamber in presence of nitrogen for 1 h.

X-ray diffraction (XRD) analysis is performed to identify the different phases, crystallinity, crystallite size and residual stresses appeared in the nitrided Al-alloy samples. X-ray diffractometer is operated at the voltage of 40 kV and current of 40 mA with Cu $K\alpha_1$ radiation ($\lambda$ = 1.540598 Å) source. The surface morphology of untreated and treated samples is demonstrated with the help of field emission JSM-5600 scanning electron microscope (SEM) operated at 10 kV for the magnification of 10 K. Micro indentation measurements are also performed to test the mechanical strength of the nitrided aluminum alloy samples using Wilson Wolport 401 MVD™ Vickers micro hardness tester.

# 3. RESULTS AND DISCUSSION

## 3.1 LANGMUIR PROBE MEASUREMENTS

**Fig. 2 shows the typical EEDF as a function of electron energy for 2 mbar pressure of nitrogen and nitrogen-argon mixture plasma. It is calculated by taking second derivative of electron saturation current with respect to probe voltage. This is usually referred to as the Druyvestyn method [21,22] given by the expression,**

$$f_E(V) = \frac{-4}{Ae^2}\left(\frac{m_e(V_p - V)}{2e}\right)^{1/2}\frac{d^2 I_{se}(V)}{dV^2} \quad (1)$$

**where $f_E(V)$, $V_p$, $A$, $I_{se}$, $m_e$ and $e$ are the electron energy distribution as a function of probe voltage, the plasma potential, probe area, electron saturation current, electronic mass and electronic charge respectively.**

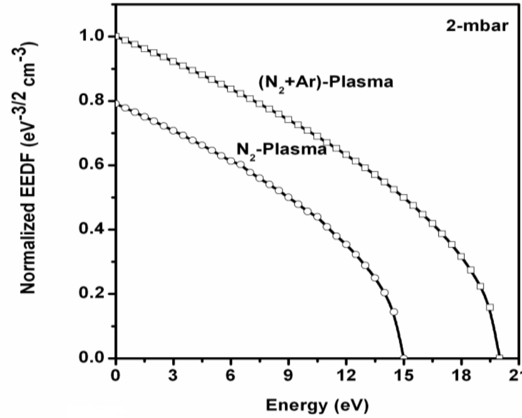


**Fig. 2: Variation of electron energy distribution function (EEDF) as a function of energy at 2 mbar filling gas ($N_2$) pressure and $N_2$-Ar mixture plasma.**

**EEDF in nitrogen-argon mixture inferred a distinct high-energy component which is most likely the result of high-energy secondary electron emission [23]. A typical EEDF for both plasmas at single pressure (2 mbar) is presented because EEDF decreases with increasing filling gas pressure which is agreed well with the previous data [23,24]. Figs. 3 and 4 show the electron temperature (eV) and electron number density ($cm^{-3}$) as a function**

of filling pressures respectively. It is observed that electron temperature and electron density is decreased with the increase of filling gas (nitrogen) pressure. Argon mixing in nitrogen plasma leads to a significant changes in plasma parameters. It is observed that electron temperature decreases while electron density increases more rapidly with nitrogen-argon mixture filling pressures [5]. In glow discharges, the electrons are more energetic than ions which are basically responsible for the most of reactions in plasma. When pressure of nitrogen gas in the chamber increases, it increases number of collisions between electrons and plasma species causing the transfer of energy from the electrons to gas particles which lowers the electron temperature. Therefore, there is decrease in ionization process and consequently the electron density [7,20].

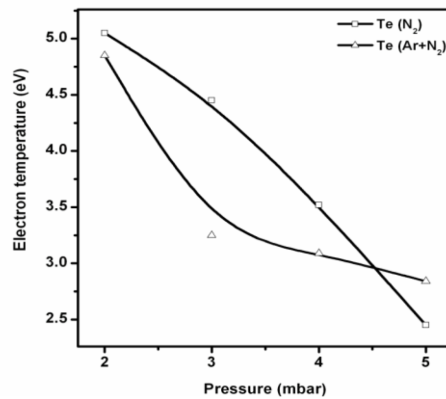


Fig. 3: Variations of electron temperature as a function of filling gas ($N_2$ and $N_2$-Ar plasma) pressure.

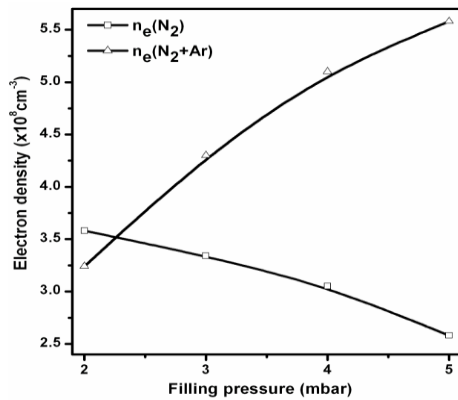


Fig. 4: Variations of electron density as a function of filling gas ($N_2$ and $N_2$-Ar plasma) pressure.

With the addition of argon gas, there is an increase in electron density which leads to higher electron-electron collision frequency and always tends to deplete electrons in the “hot tail” results in the decrease of electron temperature. At higher pressures, nitrogen ion production decreases owing to the collisional thermalization with argon [5]. At 2 mbar pressures, more energetic electrons are produced compared with other filling pressures. Therefore, only this pressure is preferred for nitridation of aluminum alloy. It is reported that increasing values of nitrogen argon ratio imply a reduction in the argon ion density in the plasma which consequently decrease the argon ion bombardment forming layer with lower nitrogen content and thus affecting the chemical composition of AIN surface layer [26].

## 3.2 SURFACE CHARACTERIZATION

### 3.2.1 X-ray diffraction (XRD) analysis

Fig. 5 shows the XRD spectra of untreated and nitrided samples of aluminum alloy for 2 mbar pressure of nitrogen as well as nitrogen-argon mixture for different processing time durations. The untreated sample of aluminum alloy has two major diffraction peaks corresponding to Al (111) and Al (200) planes confirming the face centered cubic (fcc) structure of aluminum. After nitriding, diffraction peaks corresponding to Al (111) and Al (200) planes along with AIN (111) and AIN (200) are observed which is due to the incorporation of nitrogen in aluminum matrix. Significant difference is observed in relative intensities as well as broadening of aluminum and aluminum nitride (AIN) diffraction peaks which is due to the improvement in their crystallinity by the diffusion of nitrogen atoms or ions in aluminum matrix [27,28]. However, XRD patterns reveal that the main phase in the deposited surface layer is cubic AIN. The growth of nitrided surface layer depends on nitriding time which is agreed well with the previous data [15,29]. Additionally, AIN peaks are obtained for both nitrogen and nitrogen-argon plasma.

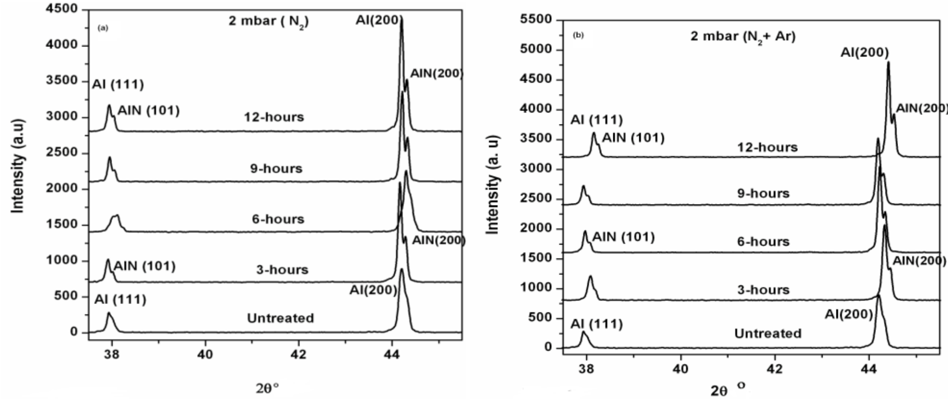


**Fig. 5: X-ray diffraction patterns of treated samples for different processing time at 2 mbar pressure of (a) $N_2$ (b) $N_2$-Ar mixture.**

**With argon gas mixing in nitrogen plasma, sputtering yield increases resulting in the increase of growth rate of surface layer. Use of nitrogen-argon mixtures in reactive nitride growth would allow energetic argon species to be used for enhancement of surface reaction and diffusion [9]. It has been demonstrated both experimentally [9,29] and theoretically [30] that the kinetic energy of colliding ions and neutrals can increase the surface diffusion and chemical reaction thereby enhances the growth of surface layer. Diffraction peaks for 12 h of processing time are shifted more toward higher angle compared with untreated and treated samples for other processing time durations. This is due to a more distortion relative to face centered cubic symmetry of lattice [29] or it may depend on various factors such as lattice structure, crystallite size, chemical composition and defect density or deformation causing due to the diffusion of nitrogen in aluminum matrix [31]. No peak of Mg is observed in XRD spectra [32] because of its low concentration. The peaks position of fcc aluminum are very close to that of fcc AlN confirming the presence of AlN (111) and AlN (200) phases which appear at the shoulder of Al (111) and Al (200) reflection planes [33]. The peaks location and intensity of Al and AlN phase changes with nitrogen concentration in the nitrided surface layer. The AlN formation may also be enhanced in the presence of alloy element such as magnesium (Mg) [4,28,34]. Magnesium in the alloy has affinity to oxygen, thereby forming magnesium oxide (MgO) which has lower surface binding**

**energy and is therefore easier to sputter [4,32] which plays an important role to increase the growth behavior of AlN surface layer. As investigated by the researchers [4,32], the growth rate of AlN surface layer increases with magnesium content in the aluminum alloy even in the presence of natural oxide on the aluminum sample surface.**

**Fig. 6 shows the variation in crystallite size of Al (111) plane as a function of processing time at 2 mbar pressure (both for nitrogen and nitrogen-argon mixture) which is measured by using Scherrer's formula [7]. It is found that the crystallite size of Al (111) plane decreases with nitriding time which is due to the diffusion of nitrogen atoms or ions interstitially. The variation in crystallite sizes is observed for different processing time durations both for nitrogen and nitrogen-argon mixture. Decrease in crystallite size and increase in peaks broadening are the factors that contribute very efficiently to the densification of surface layer which may be influenced due to the deformation or internal stress in lattice structure [28,35]. Badawi *et. al.*, [27] reported that degree of deformation and mean life time of aluminum alloy increases with the decrease of crystallite size. However, crystallite size increases in nitrogen plasma for 9 h and in nitrogen-argon plasma for 6 h comparatively which may be due to the increase of adatom mobility, high energy strain or higher crystallinity of AlN thin layer at that nitriding time.**

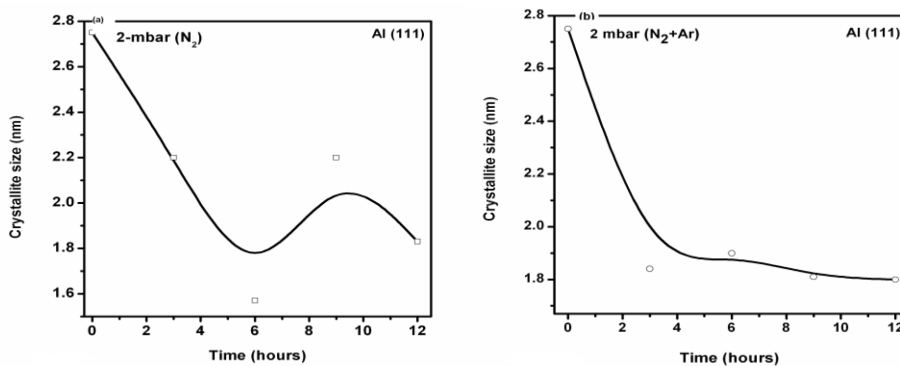


**Fig. 6: Variation of crystallite size corresponding to Al (111) reflection plane as a function of treatment time at 2 mbar pressure of (a) $N_2$ (b) $N_2$-Ar mixture.**

### 3.2.2 Residual stress measurements

**Figs. 7 and 8 show the presence of residual stresses developed in Al (111) and Al (200) planes in nitrided surface layer treated for different (3, 6, 9, 12 h) processing time at 2 mbar pressure for both nitrogen and nitrogen-argon mixture plasma. The lattice parameter determined for the nitrided surface layer at various nitriding times is found to vary linearly with the residual stress. The residual stresses produced in the treated samples are determined from XRD spectra. The residual stress produced in Al (111) and Al (200) planes is calculated by [30,35],**

$$\text{Residual stress} = \left(\frac{\Delta d}{d}\right)k \qquad (2)$$

**Where *k* is the elastic constant of aluminum alloy (*k* = $6.55\times10^4$ MPa [1]) and *Δd/d* is the strain produced in d-spacing of planes which can be determined using the following expression [30,35].**

$$\frac{\Delta d}{d} = \frac{d(observed) - d(ICSD)}{d(ICSD)} \qquad (3)$$

**All treated samples have residual stress (tensile, compressive) and the magnitude of these stresses depends on the processing conditions.**

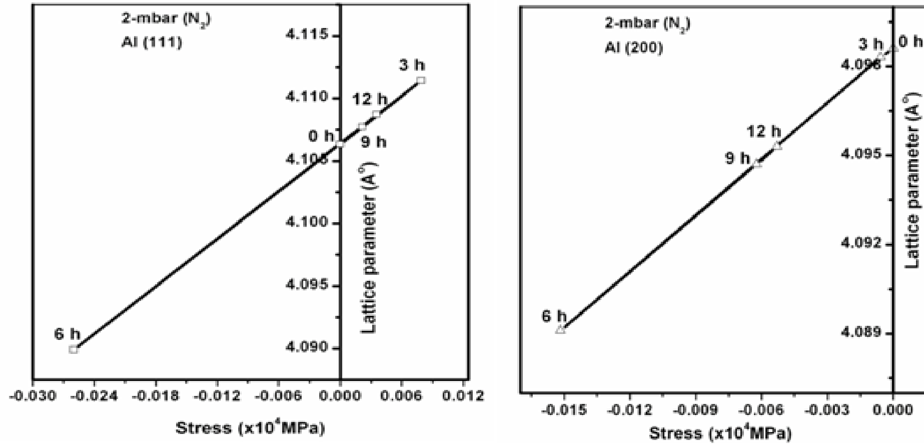


**Fig. 7: Variation of lattice parameters as a function of residual stress at 2 mbar pressure of $N_2$ for Al (111) and Al (200) reflection planes.**

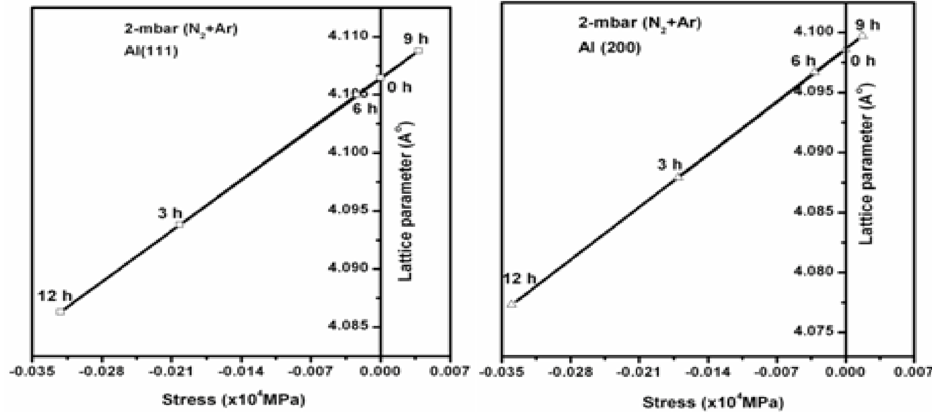


**Fig. 8:** Variation of lattice parameters as a function of residual stress at 2 mbar pressure of $N_2$-Ar mixture for Al (111) and Al (200) reflection planes.

Positive side of stress graph is tensile stress and negative side indicates the compressive stress [30]. Tensile stresses are produced in Al (111) plane at smaller processing time while for larger (6 h) processing time these stresses are transformed to compressive stresses whereas compressive stress are produced in Al (200) plane for different treatment time at 2 mbar pressure of nitrogen plasma. Due to argon mixing in nitrogen plasma, compressive stresses produced in Al (111) and Al (200) planes for smaller processing time are transformed to tensile stresses for 9 h processing time. However, maximum compressive stresses are produced when the samples are treated in argon-nitrogen plasma for 12 h. These micro structural changes are due to the incorporation of ions and ions-surface interaction mechanism [36] which may be due to the energy losses of electrons during elastic and inelastic scattering. Inelastic scattering can produce thermal effects which may be more than melting point. This leads to nitride formation by inducing localized phase transformation [36]. Elastic collisions produce primary atomic displacements of atoms which can also produce cascade collision. The cascade process can contribute to the acceleration of diffusion processes and the formation of new phases related to nitrides of Al.

It is inferred that with the addition of argon in nitrogen plasma, same behavior of residual stresses regarding to transition from compressive to tensile or tensile to compressive [37] is observed in Al (111) and Al (200) planes compared with the stresses produced during nitriding in pure nitrogen. The compressive stress is very often considered to be due to atomic peening process and sometimes as the consequence of charge particles incorporation in the surface layer. It has been reported [38] that the atomic (shot) peened surface would have a microstructure that differ significantly from that of the bulk. Present study is the direct consequence of energetic atoms or ions processing. It can be deduced that bigger crystallites with considerable stress breaks into smaller crystallite with reduce stress and better packing reduces the residual stress.

### 3.2.3 Surface Morphology

Fig. 9 shows the change in surface morphology induced by nitriding. The morphology of untreated and treated surface layers is investigated by SEM. The representative SEM pictures of samples treated for 12 h at 2 mbar pressure for both nitrogen and nitrogen-argon mixture plasma are displayed. Morphological manifestation seems to be consistent with the structural studies. The morphology of samples treated in pure nitrogen is quite different from the samples treated in nitrogen-argon mixture plasma because of different crystallite orientations.

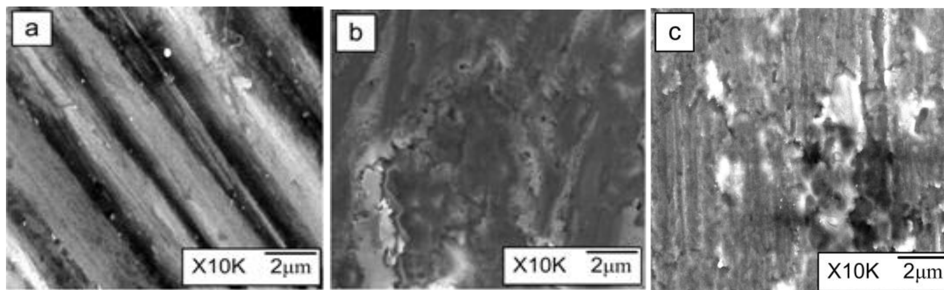


Fig. 9: SEM micrographs of untreated (a), nitrided samples for 12 h at 2 mbar filling pressure of $N_2$ (b) and $N_2$-Ar mixture (c).

Nevertheless, the effect of argon atoms or ions on grain size can be analyzed from morphological studies. With prolongation of nitriding time,

AlN particles in surface layer grow further results in the formation of coalescence [29]. It can be observed that surface layer becomes wrinkled by grooves. Further increase in nitriding time confirms the tendency of coalescence but also damaging of plane layer is observed. Beside larger processing time, high doses of nitrogen and nitrogen and nitrogen-argon mixture results in the surface swelling which increases the surface roughness [39,40]. With the addition of argon, sputtering becomes more pronounced thereby reducing the diffusion possibility to the substrate so that nitride surface layer cannot grow further. Thus, it is inferred that a certain minimum atom or ion energy is required to bring the smooth morphological structural changes in aluminum nitride surface layer.

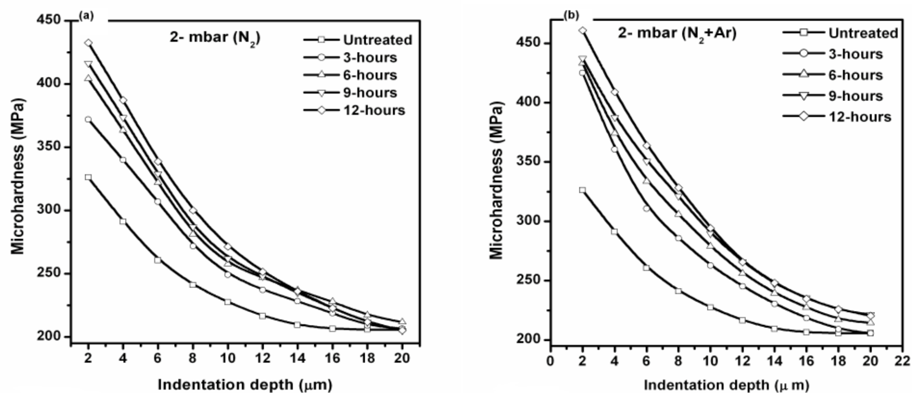


Fig. 10: Variation of surface hardness as a function of indentation depth for different time durations at 2 mbar pressure of (a) $N_2$ (b) $N_2$-Argon mixture.

### 3.2.4 Surface Hardness Measurements

Fig. 10 shows the surface micro hardness as a function of indentation depth of untreated and treated samples which is measured at different imposed loads ranging from 0.01 to 0.5 kgf for dwell time of 5 s. Hardness is the ability of a material to resist permanent penetration by much harder body. It is observed that hardness increases with the decrease of indentation depth and imposed load [4,7], suggesting the formation of the thick modified surface layer of AlN. However, the hardness increases with increasing nitriding time [3]. There is an increase of hardness after nitriding that is caused by the increase of nitrogen contents and the formation of

AlN. With increasing nitriding time, the diffusion is increased due to the locally increase of temperature, nitrides formation and nitrogen contents which results in the increase of hardness [36]. Surface hardness increases in both cases with the increase of nitriding time. However, significant increase in hardness is obtained for 12 h processing time at 2 mbar pressure of nitrogen-argon mixture plasma. Results on the effect of argon mixing show that most effective nitriding of aluminum alloy could be achieved with the addition of argon compared with nitriding in pure nitrogen plasma [41].

## 4. CONCLUSIONS

Nitrogen and nitrogen-argon mixture plasmas are characterized by using Langmuir probe. It is found that EEDF in nitrogen-argon mixture plasma is greater than in pure nitrogen plasma. Electron temperature and density decreases with increasing pressure of nitrogen plasma. However, with the addition of argon in nitrogen, electron density increases while temperature decreases with the increase of pressure which is due to the increase in electron-electron collisions. The XRD spectra of treated samples confirm the formation of cubic AlN which is due to the incorporation of nitrogen ions into substrate matrix forming the solid solution. The crystallite size decreases rapidly during 3 h to 6 h and then varies after 6 h in nitrogen plasma but almost constant for nitrogen-argon mixture plasma after 6 h. Shift of the diffraction peaks from their corresponding stress free data indicate that the tensile and compressive stresses are produced. However, compressive stress is produced in Al (200) plane for all treatment time durations in nitrogen plasma. On the other hand, the same pattern of stresses (compressive or tensile) is produced in both planes of Al when the samples are treated in both nitrogen and nitrogen-argon mixture plasma, demonstrating that same reactions are produced during gas-solid interaction phenomenon. Surface micro-hardness increases with the increase of treatment time (3, 6, 9, 12 h) for both nitrogen and nitrogen-argon mixture plasma. Significant increase in hardness and compressive stress is obtained at a pressure of 2 mbar of nitrogen-argon mixture

**plasma for treatment time of 12 h. The XRD, SEM and hardness measurements reveal that argon mixing is an effective way to enhance the production of active species and more favorable for infusion of nitrogen in aluminum alloy matrix. In addition, the argon in the gas mixture causes the rapid growth of compound layer.**

## REFERENCES


1. R. B. Ross, Metallic Materials Specification Hand Book, 4th Edition, Chapman and Hall, (1992).
2. M. Sadiq, S. Ahmad, A. Waheed and M. Zakaullah, Plasma Source Sci. Technol., 15 (2006) 295.
3. Y. Sun, J. Alloys & Comp., 351 (2003) 241.
4. H. Spies, B. Reinhold and K. Wilsdorf, Surf. Eng., 17 (1) (2001) 41.
5. Y. Pu, Z. Guo, Z. Dekang, J. Ma, Z. Guan, G. Zhang and W. En-Ge, Pure Appl. Chem., 74(3) (2002) 459.
6. C. Chetan, Samant, A. D. Rupji, S. V. Gogawale, D. C. Kothari and V. H. Kulkarni, Surf. Coat Technol., 158 (2002) 658.
7. M. S. Shah, M. Saleem, R. Ahmad, M. Zakaullah, A. Qayyum and G. Murtaza, J. Mater. Process Technol., 199 (2008) 363.
8. Z. Jianxin, H. Jining, D. Yanchun, L. Xiangzhi and Y. Dianran, J. Mater. Process Technol., 197 (2008) 31.
9. Z. Y. Fan and N. Newman, Appl. Phys. Lett., 73 (1998) 456.
10. S. V. Bagul, S. D. Chavhan and S. Ramphal, J. Phys. & Chem. Solids, 68 (2007) 1623.
11. M. U. Kamachi, H. S. Khatak, R. Baldev and M. Uhlemann, Mat. Manufact. Process, 19 (1) (2004) 61.
12. A. Alsaran and A. Çelik, Mater. Charact., 47 (2001) 207.
13. M Karakan, A Alsaran and A Çelik, Mater. Charact., 49 (2003) 241.
14. T. Fitz and W. Moller, J. Appl. Phys., 92 (11) (2002) 6862.
15. M. Moradshahi, T. Tavakoli, S. Amiri and S. Shayeganmchr, Surf. Coat. Technol., 201 (2006) 567.
16. F. A. Haas, A. Goodyear and N. S. J. Braithwaite, Plasma Sources Sci. Technol., 7 (1998) 471.

17. F. A. Haas and N. S. J. Braithwaite, Appl. Phys. Lett., 74 (1999) 338.
18. H. Shindo, T. Urayama, T. Fujii, Y. Horiike and S. Fujii, Jpn. J. Appl. Phys., 38 (1999) L1066.
19. M. Nisha, K. J. Saji, R. S. Ajimsha, N. V. Joshy and M. K. Jayaraj, J. Appl. Phys., 99 (2006) 033304-1.
20. A. Qayyum, M. Ikram, M. Zakaullah, A. Waheed, G. Murtaza, R. Ahmad, A. Majeed, N. A. D. Khattak, K. Mansoor and K. A. Chaudhry, Int. J. Mod. Phys., B 17 (2003) 1.
21. M. J. Druyvesteyn, Z. Phys., 64 (1930) 781.
22. S. Miyamoto, F. Kanayama, T. Mune and H. Horiike, Nucl. Fusion, 46 (2006) S313.
23. H. Singh and D. B. Graves, J. Appl. Phys., 87(9) (2000) 4098.
24. M. M. Turner, R. A. Doyle and M. B. Hopkins, Appl. Phys. Lett., 62 (1993) 3247.
25. A. Grill, Cold Plasma in Materials Fabrication, IEEE Press, New York, (1993).
26. H. X. Ming, N. Baker, B. A. Kehler, K. C. Walter, M. Nastasi and Y. Nakamura, J. Vac. Sci. Technol., A 18 (1) (2002) 30.
27. E. Badawi, M. A. Abdel-Rahman, S. A. Mahmoud and A. A. Ramadan, Turk. J. Phys., 24 (2000) 543.
28. S. Ohira, K. Hiei and M. Iwaki, Nucl. Instrum. Method Phys. Res., B 32 (1988) 66.
29. L. Wang, S. Ji and J. Sun, Surf. Coat. Technol., 200 (2006) 5067.
30. R. S. Rawat, P. Arun, A. G. Vedeshwar, P. Lee and S. Lee, J. Appl. Phys., 95 (2004) 7725.
31. S. J. Ji, L. Wang, J. C. Sun and Z. K. Hei, Surf. Coat. Technol., 195 (2005) 81.
32. U. Figueroa, O. Salas and J. Oseguera, Thin Solid Films, 469 (2004) 295.
33. T. Telbizova, S. Parascandola, F. Prokert, N. P. Barradas, E. Richter and W. Moller, Surf. Coat. Technol., 142 (2001) 1028.
34. S. Gredelj, A. R. Gerson, S. Kumar and G. P. Cavallaro, Appl. Surf. Sci., 199 (2002) 183.
35. P. Tyagi and A. G. Vedeshwar, Phys. Rev., B 66 (2002) 075422-1.

36. M. W. Thompson, Defects and Radiation Damage in Metals, University Press, Cambrigde, (1969).

37. G. Knuyt, W. Lauwerens and L. M. Stals, Thin Solid Films, 370 (2000) 232.

38. Z. D. Xiang and P. K. Datta, Scripta Materialia, 55 (2006) 1151.

39. S. Gredelj, A. R. Gerson, S. Kumar and G. P. Cavallaro, Appl. Surf. Sci., 174 (2001) 240.

40. M. Quast, P. Mayr and H. R. Stock, Surf. Coat. Technol., 120/121 (1999) 244.

41. A. Zhecheva, S. Wei, S. Malinov and Adrian Long, Surf. Coat. Technol., 200 (2005) 2192.

PK ISSN 0022- 2941; CODEN JNSMAC
Vol. 49, No.1 & 2 (April & October 2009) PP 1-17

# CHARACTERIZATION AND EFFECT OF ARGON-NITROGEN PLASMA ON NITRIDATION OF ALUMINUM ALLOY

M. S. SHAH, N. KHAN AND R. AHMAD

Department of Physics, Government College University, 54000 Lahore, Pakistan
E-mail Addresses: ms_shah_sgd@yahoo.com

(Received: February 10, 2011)

**ABSTRACT:** Langmuir probe is used to determine the plasma parameters for the mixture of nitrogen-argon gases using ac generated plasma source. Results reveal that argon mixing in nitrogen plasma is an effective mode to increase electron density. Samples are exposed for 3, 6, 9 and 12 h for constant pressure (2 mbar) and electrical input power (100 W). Nitriding of aluminum alloy is performed in a mixture of argon and nitrogen plasma (1:1) plasmas, to investigate the effect of argon mixing on its surface properties. The analysis is carried out by using x-ray diffractometer (XRD), scanning electron microscopy (SEM) and Vickers micro hardness tester to investigate surface properties of the treated samples. XRD results exhibit the formation of cubic AlN thin surface layer by reactive ac sputtering with argon as a sputtering gas and nitrogen as a reactive gas. Moreover, significant increase in surface hardness is found when the sample is treated for 12 h in nitrogen-argon plasma.

**Keywords:** 50 Hz ac discharge, Plasma characterization, Nitriding, X-ray diffraction.

## 1. INTRODUCTION

Aluminum and its alloys have extensive industrial applications due to their light weight, high strength to weight ratio, good corrosion resistance and formability along with good electrical and thermal conductivities [1,2]. Aluminum nitrides are also widely investigated as an electronic and optoelectronic material as well as its favorable thermal, acoustic, optical and electrical properties. However, low surface hardness and wear resistance limit their applications in automotive, aero space and electronic industry. These surface properties can be improved by nitriding the aluminum and aluminum alloy. It is very difficult to form AlN by conventional techniques due to the formation of protective pre-existed oxide layer on the surface of aluminum alloy. The thin oxide layer prevents

**the diffusion of nitrogen into the aluminum matrix. In plasma nitriding, this oxide layer can be removed by transfer of sufficient energy during the bombardment of energetic particles [3]. The subsequent transfer of nitrogen from surface to interior of the material to form a nitrided layer is normally governed by diffusion. However, oxide layer can also be removed more effectively by sputtering prior or during nitriding with argon plasma bombardment. For this purpose argon is used to sputter the oxide layer [4,5], clean the surface and facilitate the diffusion of nitrogen into the aluminum matrix [6]. Plasma nitriding is widely used to enhance the mechanical and chemical properties of materials [7-11]. It is primarily used to enhance fatigue strength, surface hardness, wear and corrosion resistance without affecting bulk properties of materials [12,13]. Low temperature (<500$^{o}$ C) plasma nitriding is highly desirable [14], for nitrogen enriched diffusion layer with significant depth and high hardness while at higher temperatures, the deposited surface layers often show poor adhesion to the substrate [4]. The growth of nitrided surface layer follows the diffusion law and increase in layer thickness is attributed with increasing treatment time [15].**

**Another consideration in plasma processing is the production of active species and these are determined by the electron energy. Several techniques have been proposed to alter electron temperature and density [16-18]. It is found that the mixing of inert gas (Ar) in nitrogen plasma is an effective way to change the plasma parameters such as electron temperature and electron density [5]. Electron energy distribution function (EEDF), electron temperature and electron number density are important plasma parameters which influence the production of active species by inelastic collisions, plasma reactions and plasma surface interactions. Therefore, Langmuir probe [19,20] is employed for obtaining information regarding plasma parameters.**

**This paper reports the 50 Hz ac generated glow discharges which are economically attractive in industry due to their simplicity and cost-effectiveness. The present study concentrates on the effects of argon on**

**plasma parameters regarding EEDF, electron temperature, electron density and consequently on nitriding behavior of aluminum alloy with influence of processing time. This work also focused on the improvement of mechanical properties by investigating the dependence of structural and compositional properties including crystallographic structure, surface morphology and surface hardness of samples treated for different times. The influence of surface layer composition on the residual stress, hardness and tribological properties are also examined.**

## 2. EXPERIMENTAL PROCEDURES

**Aluminum alloy ($AlMg_2Si$) specimen of dimension 9×9×3 $mm^3$ are polished using SiC abrasive paper from coarse to fine grade (220 ~ 1000) on Stuers Knuth-Rotor-3 polishing machine and then cleaned ultrasonically. Nitriding of aluminum alloy is performed in cold plasma device shown in Fig. 1. It consists of a stainless steel vacuum chamber having diameter and height of 32 cm. Two circular stainless steel electrodes having 14 cm diameter and thickness of 2 cm each are adjusted in chamber in a capacitive configuration of spacing 3 cm.**

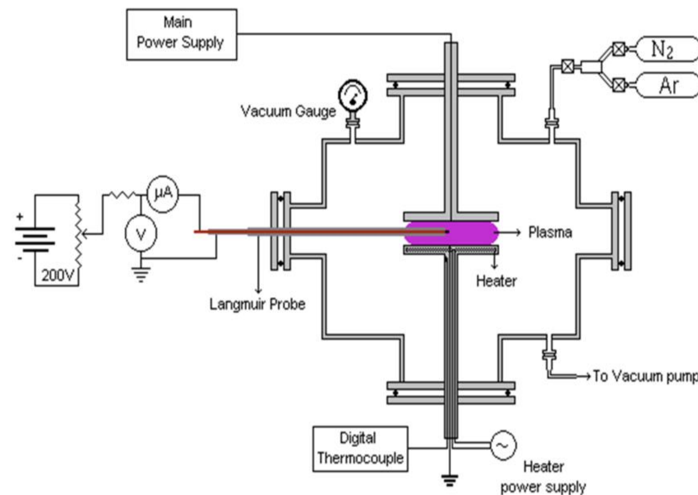


**Fig. 1: Experimental setup of the plasma nitridation system.**

The chamber is evacuated down to a pressure of $1\times10^{-2}$ mbar using a rotary vane pump. The working pressure of nitrogen and nitrogen-argon plasma is 2 mbar during nitridation process. The pressure of the chamber is measured using capsule type vacuum gauge. A 100 W ac power output from a variac transformer is applied to the top electrode through an inductive load which limits the currents during the discharge. The samples are placed on the bottom electrode which is grounded. The inlet and outlet valves are adjusted so as to maintain the desired pressure in the chamber. Langmuir probe is used as plasma diagnostic due to its easy and simple execution compared to other plasma diagnostics. Probe current is measured for DC bias voltages swept from -100 V to +100 V. For probe measurements, I-V characteristics are recorded by varying pressure from 2 mbar to 5 mbar by keeping power constant of 100 W.

Four samples are subjected to nitrogen plasma at 2-mbar pressure for 3, 6, 9, and 12 h time durations. A second set of four samples is also exposed to nitrogen-argon mixture plasma with same plasma processing parameters. During nitriding process, the temperature of the samples is maintained at 250$^{o}$C by using thermocouple. After nitriding, the samples are cooled down in the chamber in presence of nitrogen for 1 h.

X-ray diffraction (XRD) analysis is performed to identify the different phases, crystallinity, crystallite size and residual stresses appeared in the nitrided Al-alloy samples. X-ray diffractometer is operated at the voltage of 40 kV and current of 40 mA with Cu $K\alpha_1$ radiation ($\lambda$ = 1.540598 Å) source. The surface morphology of untreated and treated samples is demonstrated with the help of field emission JSM-5600 scanning electron microscope (SEM) operated at 10 kV for the magnification of 10 K. Micro indentation measurements are also performed to test the mechanical strength of the nitrided aluminum alloy samples using Wilson Wolport 401 MVD$^{TM}$ Vickers micro hardness tester.

# 3. RESULTS AND DISCUSSION

## 3.1 LANGMUIR PROBE MEASUREMENTS

**Fig. 2 shows the typical EEDF as a function of electron energy for 2 mbar pressure of nitrogen and nitrogen-argon mixture plasma. It is calculated by taking second derivative of electron saturation current with respect to probe voltage. This is usually referred to as the Druyvestyn method [21,22] given by the expression,**

$$f_E(V) = \frac{-4}{Ae^2}\left(\frac{m_e(V_p - V)}{2e}\right)^{1/2} \frac{d^2 I_{se}(V)}{dV^2} \quad \textbf{(1)}$$

**where $f_E(V)$, $V_p$, $A$, $I_{se}$, $m_e$ and $e$ are the electron energy distribution as a function of probe voltage, the plasma potential, probe area, electron saturation current, electronic mass and electronic charge respectively.**

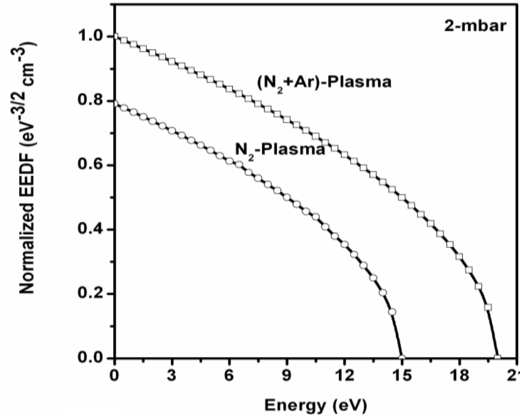


**Fig. 2: Variation of electron energy distribution function (EEDF) as a function of energy at 2 mbar filling gas ($N_2$) pressure and $N_2$-Ar mixture plasma.**

**EEDF in nitrogen-argon mixture inferred a distinct high-energy component which is most likely the result of high-energy secondary electron emission [23]. A typical EEDF for both plasmas at single pressure (2 mbar) is presented because EEDF decreases with increasing filling gas pressure which is agreed well with the previous data [23,24]. Figs. 3 and 4 show the electron temperature (eV) and electron number density ($cm^{-3}$) as a function**

of filling pressures respectively. It is observed that electron temperature and electron density is decreased with the increase of filling gas (nitrogen) pressure. Argon mixing in nitrogen plasma leads to a significant changes in plasma parameters. It is observed that electron temperature decreases while electron density increases more rapidly with nitrogen-argon mixture filling pressures [5]. In glow discharges, the electrons are more energetic than ions which are basically responsible for the most of reactions in plasma. When pressure of nitrogen gas in the chamber increases, it increases number of collisions between electrons and plasma species causing the transfer of energy from the electrons to gas particles which lowers the electron temperature. Therefore, there is decrease in ionization process and consequently the electron density [7,20].

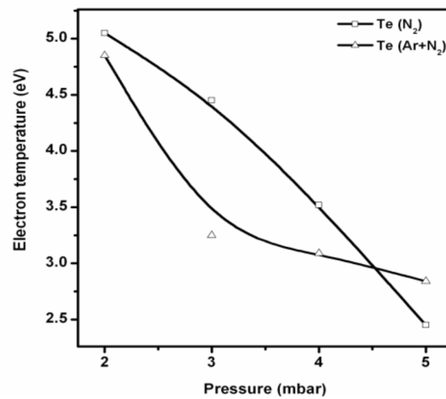


Fig. 3: Variations of electron temperature as a function of filling gas ($N_2$ and $N_2$-Ar plasma) pressure.

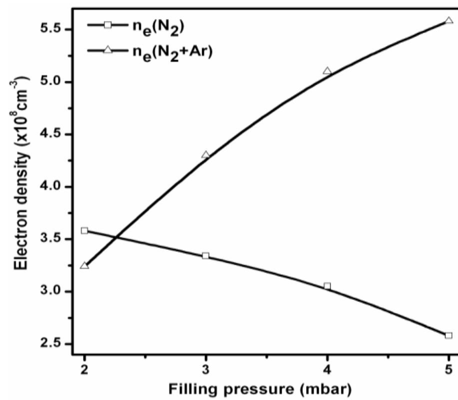


Fig. 4: Variations of electron density as a function of filling gas ($N_2$ and $N_2$-Ar plasma) pressure.

With the addition of argon gas, there is an increase in electron density which leads to higher electron-electron collision frequency and always tends to deplete electrons in the "hot tail" results in the decrease of electron temperature. At higher pressures, nitrogen ion production decreases owing to the collisional thermalization with argon [5]. At 2 mbar pressures, more energetic electrons are produced compared with other filling pressures. Therefore, only this pressure is preferred for nitridation of aluminum alloy. It is reported that increasing values of nitrogen argon ratio imply a reduction in the argon ion density in the plasma which consequently decrease the argon ion bombardment forming layer with lower nitrogen content and thus affecting the chemical composition of AlN surface layer [26].

## 3.2 SURFACE CHARACTERIZATION

### 3.2.1 X-ray diffraction (XRD) analysis

Fig. 5 shows the XRD spectra of untreated and nitrided samples of aluminum alloy for 2 mbar pressure of nitrogen as well as nitrogen-argon mixture for different processing time durations. The untreated sample of aluminum alloy has two major diffraction peaks corresponding to Al (111) and Al (200) planes confirming the face centered cubic (fcc) structure of aluminum. After nitriding, diffraction peaks corresponding to Al (111) and Al (200) planes along with AlN (111) and AlN (200) are observed which is due to the incorporation of nitrogen in aluminum matrix. Significant difference is observed in relative intensities as well as broadening of aluminum and aluminum nitride (AlN) diffraction peaks which is due to the improvement in their crystallinity by the diffusion of nitrogen atoms or ions in aluminum matrix [27,28]. However, XRD patterns reveal that the main phase in the deposited surface layer is cubic AlN. The growth of nitrided surface layer depends on nitriding time which is agreed well with the previous data [15,29]. Additionally, AlN peaks are obtained for both nitrogen and nitrogen-argon plasma.

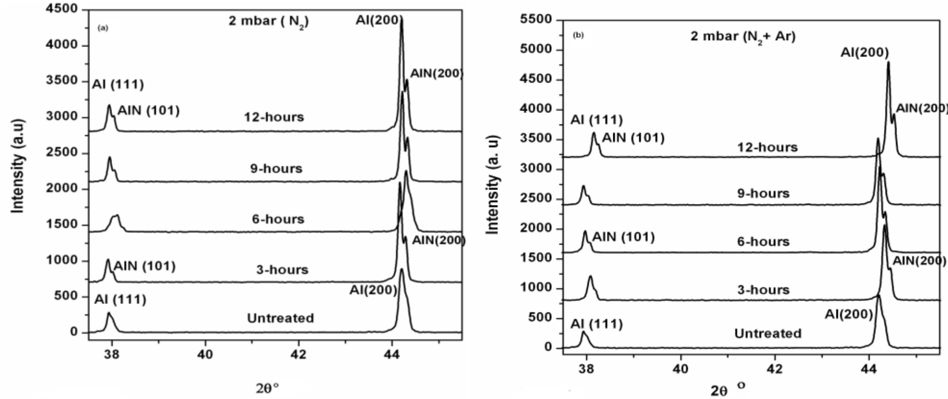


Fig. 5: X-ray diffraction patterns of treated samples for different processing time at 2 mbar pressure of (a) $N_2$ (b) $N_2$-Ar mixture.

With argon gas mixing in nitrogen plasma, sputtering yield increases resulting in the increase of growth rate of surface layer. Use of nitrogen-argon mixtures in reactive nitride growth would allow energetic argon species to be used for enhancement of surface reaction and diffusion [9]. It has been demonstrated both experimentally [9,29] and theoretically [30] that the kinetic energy of colliding ions and neutrals can increase the surface diffusion and chemical reaction thereby enhances the growth of surface layer. Diffraction peaks for 12 h of processing time are shifted more toward higher angle compared with untreated and treated samples for other processing time durations. This is due to a more distortion relative to face centered cubic symmetry of lattice [29] or it may depend on various factors such as lattice structure, crystallite size, chemical composition and defect density or deformation causing due to the diffusion of nitrogen in aluminum matrix [31]. No peak of Mg is observed in XRD spectra [32] because of its low concentration. The peaks position of fcc aluminum are very close to that of fcc AlN confirming the presence of AlN (111) and AlN (200) phases which appear at the shoulder of Al (111) and Al (200) reflection planes [33]. The peaks location and intensity of Al and AlN phase changes with nitrogen concentration in the nitrided surface layer. The AlN formation may also be enhanced in the presence of alloy element such as magnesium (Mg) [4,28,34]. Magnesium in the alloy has affinity to oxygen, thereby forming magnesium oxide (MgO) which has lower surface binding

energy and is therefore easier to sputter [4,32] which plays an important role to increase the growth behavior of AlN surface layer. As investigated by the researchers [4,32], the growth rate of AlN surface layer increases with magnesium content in the aluminum alloy even in the presence of natural oxide on the aluminum sample surface.

Fig. 6 shows the variation in crystallite size of Al (111) plane as a function of processing time at 2 mbar pressure (both for nitrogen and nitrogen-argon mixture) which is measured by using Scherrer's formula [7]. It is found that the crystallite size of Al (111) plane decreases with nitriding time which is due to the diffusion of nitrogen atoms or ions interstitially. The variation in crystallite sizes is observed for different processing time durations both for nitrogen and nitrogen-argon mixture. Decrease in crystallite size and increase in peaks broadening are the factors that contribute very efficiently to the densification of surface layer which may be influenced due to the deformation or internal stress in lattice structure [28,35]. Badawi *et. al.*, [27] reported that degree of deformation and mean life time of aluminum alloy increases with the decrease of crystallite size. However, crystallite size increases in nitrogen plasma for 9 h and in nitrogen-argon plasma for 6 h comparatively which may be due to the increase of adatom mobility, high energy strain or higher crystallinity of AlN thin layer at that nitriding time.

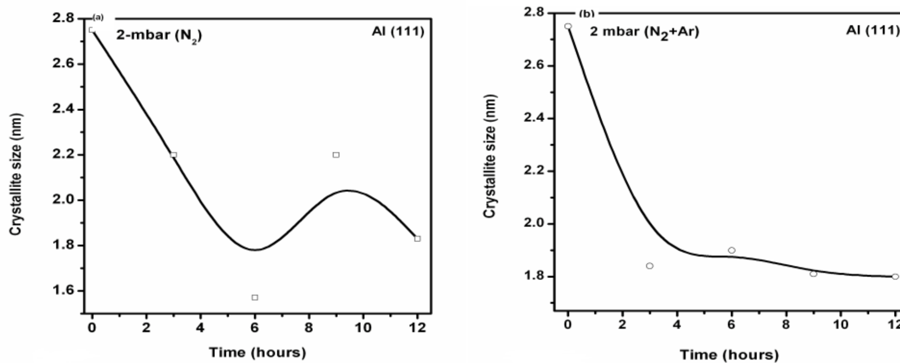


Fig. 6: Variation of crystallite size corresponding to Al (111) reflection plane as a function of treatment time at 2 mbar pressure of (a) $N_2$ (b) $N_2$-Ar mixture.

### 3.2.2 Residual stress measurements

**Figs. 7 and 8 show the presence of residual stresses developed in Al (111) and Al (200) planes in nitrided surface layer treated for different (3, 6, 9, 12 h) processing time at 2 mbar pressure for both nitrogen and nitrogen-argon mixture plasma. The lattice parameter determined for the nitrided surface layer at various nitriding times is found to vary linearly with the residual stress. The residual stresses produced in the treated samples are determined from XRD spectra. The residual stress produced in Al (111) and Al (200) planes is calculated by [30,35],**

$$\text{Residual stress} = \left(\frac{\Delta d}{d}\right)k \tag{2}$$

**Where *k* is the elastic constant of aluminum alloy (*k* = $6.55\times10^4$ MPa [1]) and *Δd/d* is the strain produced in d-spacing of planes which can be determined using the following expression [30,35].**

$$\frac{\Delta d}{d} = \frac{d(observed) - d(ICSD)}{d(ICSD)} \tag{3}$$

**All treated samples have residual stress (tensile, compressive) and the magnitude of these stresses depends on the processing conditions.**

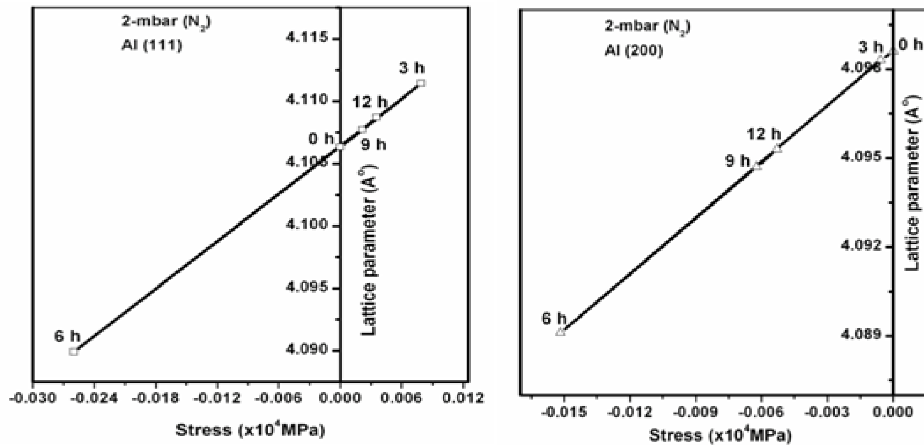


**Fig. 7: Variation of lattice parameters as a function of residual stress at 2 mbar pressure of $N_2$ for Al (111) and Al (200) reflection planes.**

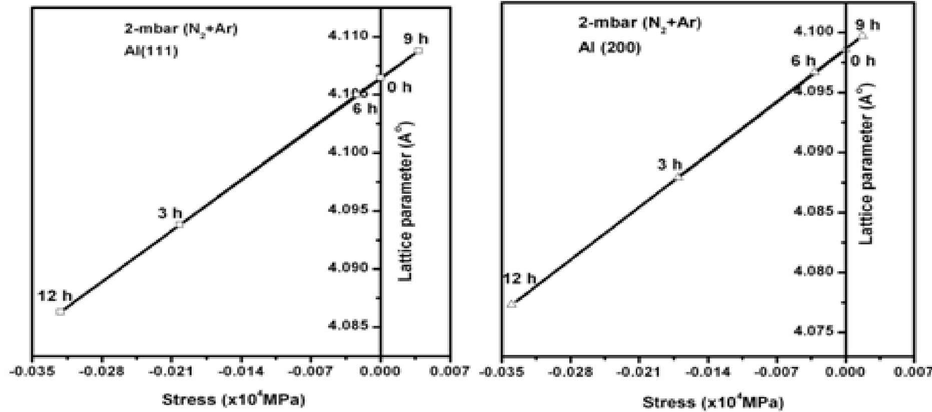


**Fig. 8:** **Variation of lattice parameters as a function of residual stress at 2 mbar pressure of $N_2$-Ar mixture for Al (111) and Al (200) reflection planes.**

**Positive side of stress graph is tensile stress and negative side indicates the compressive stress [30]. Tensile stresses are produced in Al (111) plane at smaller processing time while for larger (6 h) processing time these stresses are transformed to compressive stresses whereas compressive stress are produced in Al (200) plane for different treatment time at 2 mbar pressure of nitrogen plasma. Due to argon mixing in nitrogen plasma, compressive stresses produced in Al (111) and Al (200) planes for smaller processing time are transformed to tensile stresses for 9 h processing time. However, maximum compressive stresses are produced when the samples are treated in argon-nitrogen plasma for 12 h. These micro structural changes are due to the incorporation of ions and ions-surface interaction mechanism [36] which may be due to the energy losses of electrons during elastic and inelastic scattering. Inelastic scattering can produce thermal effects which may be more than melting point. This leads to nitride formation by inducing localized phase transformation [36]. Elastic collisions produce primary atomic displacements of atoms which can also produce cascade collision. The cascade process can contribute to the acceleration of diffusion processes and the formation of new phases related to nitrides of Al.**

It is inferred that with the addition of argon in nitrogen plasma, same behavior of residual stresses regarding to transition from compressive to tensile or tensile to compressive [37] is observed in Al (111) and Al (200) planes compared with the stresses produced during nitriding in pure nitrogen. The compressive stress is very often considered to be due to atomic peening process and sometimes as the consequence of charge particles incorporation in the surface layer. It has been reported [38] that the atomic (shot) peened surface would have a microstructure that differ significantly from that of the bulk. Present study is the direct consequence of energetic atoms or ions processing. It can be deduced that bigger crystallites with considerable stress breaks into smaller crystallite with reduce stress and better packing reduces the residual stress.

### 3.2.3 Surface Morphology

Fig. 9 shows the change in surface morphology induced by nitriding. The morphology of untreated and treated surface layers is investigated by SEM. The representative SEM pictures of samples treated for 12 h at 2 mbar pressure for both nitrogen and nitrogen-argon mixture plasma are displayed. Morphological manifestation seems to be consistent with the structural studies. The morphology of samples treated in pure nitrogen is quite different from the samples treated in nitrogen-argon mixture plasma because of different crystallite orientations.

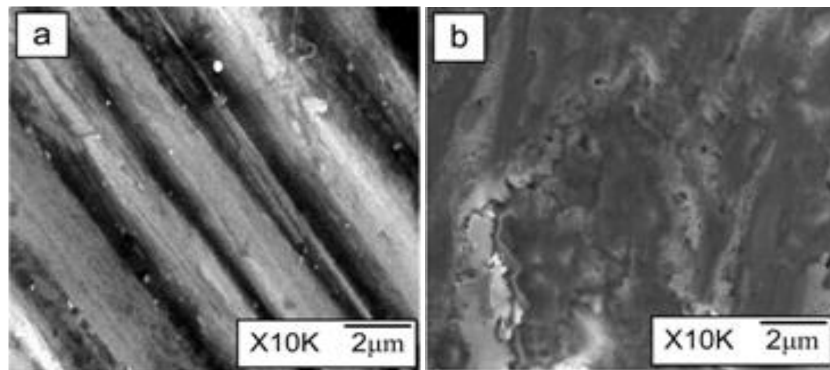


Fig. 9: SEM micrographs of untreated (a), nitrided samples for 12 h at 2 mbar filling pressure of $N_2$ (b) and $N_2$-Ar mixture (c).

Nevertheless, the effect of argon atoms or ions on grain size can be analyzed from morphological studies. With prolongation of nitriding time, AlN particles in surface layer grow further results in the formation of coalescence [29]. It can be observed that surface layer becomes wrinkled by grooves. Further increase in nitriding time confirms the tendency of coalescence but also damaging of plane layer is observed. Beside larger processing time, high doses of nitrogen and nitrogen and nitrogen-argon mixture results in the surface swelling which increases the surface roughness [39,40]. With the addition of argon, sputtering becomes more pronounced thereby reducing the diffusion possibility to the substrate so that nitride surface layer cannot grow further. Thus, it is inferred that a certain minimum atom or ion energy is required to bring the smooth morphological structural changes in aluminum nitride surface layer.

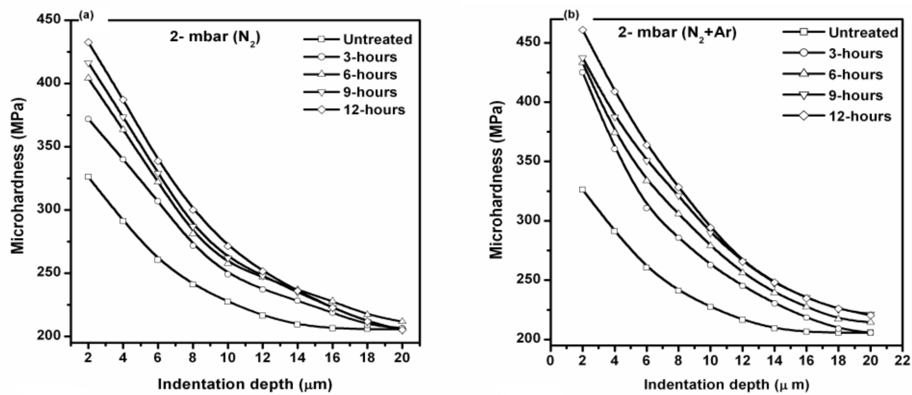


Fig. 10: Variation of surface hardness as a function of indentation depth for different time durations at 2 mbar pressure of (a) $N_2$ (b) $N_2$-Argon mixture.

### 3.2.4 Surface Hardness Measurements

Fig. 10 shows the surface micro hardness as a function of indentation depth of untreated and treated samples which is measured at different imposed loads ranging from 0.01 to 0.5 kgf for dwell time of 5 s. Hardness is the ability of a material to resist permanent penetration by much harder body. It is observed that hardness increases with the decrease of indentation depth and imposed load [4,7], suggesting the formation of the thick modified surface layer of AlN. However, the hardness increases with

increasing nitriding time [3]. There is an increase of hardness after nitriding that is caused by the increase of nitrogen contents and the formation of AlN. With increasing nitriding time, the diffusion is increased due to the locally increase of temperature, nitrides formation and nitrogen contents which results in the increase of hardness [36]. Surface hardness increases in both cases with the increase of nitriding time. However, significant increase in hardness is obtained for 12 h processing time at 2 mbar pressure of nitrogen-argon mixture plasma. Results on the effect of argon mixing show that most effective nitriding of aluminum alloy could be achieved with the addition of argon compared with nitriding in pure nitrogen plasma [41].

## 4. CONCLUSIONS

Nitrogen and nitrogen-argon mixture plasmas are characterized by using Langmuir probe. It is found that EEDF in nitrogen-argon mixture plasma is greater than in pure nitrogen plasma. Electron temperature and density decreases with increasing pressure of nitrogen plasma. However, with the addition of argon in nitrogen, electron density increases while temperature decreases with the increase of pressure which is due to the increase in electron-electron collisions. The XRD spectra of treated samples confirm the formation of cubic AlN which is due to the incorporation of nitrogen ions into substrate matrix forming the solid solution. The crystallite size decreases rapidly during 3 h to 6 h and then varies after 6 h in nitrogen plasma but almost constant for nitrogen-argon mixture plasma after 6 h. Shift of the diffraction peaks from their corresponding stress free data indicate that the tensile and compressive stresses are produced. However, compressive stress is produced in Al (200) plane for all treatment time durations in nitrogen plasma. On the other hand, the same pattern of stresses (compressive or tensile) is produced in both planes of Al when the samples are treated in both nitrogen and nitrogen-argon mixture plasma, demonstrating that same reactions are produced during gas-solid interaction phenomenon. Surface micro-hardness increases with the increase of treatment time (3, 6, 9, 12 h) for both nitrogen and nitrogen-

argon mixture plasma. Significant increase in hardness and compressive stress is obtained at a pressure of 2 mbar of nitrogen-argon mixture plasma for treatment time of 12 h. The XRD, SEM and hardness measurements reveal that argon mixing is an effective way to enhance the production of active species and more favorable for infusion of nitrogen in aluminum alloy matrix. In addition, the argon in the gas mixture causes the rapid growth of compound layer.

## REFERENCES


1. R. B. Ross, Metallic Materials Specification Hand Book, 4th Edition, Chapman and Hall, (1992).
2. M. Sadiq, S. Ahmad, A. Waheed and M. Zakaullah, Plasma Source Sci. Technol., 15 (2006) 295.
3. Y. Sun, J. Alloys & Comp., 351 (2003) 241.
4. H. Spies, B. Reinhold and K. Wilsdorf, Surf. Eng., 17 (1) (2001) 41.
5. Y. Pu, Z. Guo, Z. Dekang, J. Ma, Z. Guan, G. Zhang and W. En-Ge, Pure Appl. Chem., 74(3) (2002) 459.
6. C. Chetan, Samant, A. D. Rupji, S. V. Gogawale, D. C. Kothari and V. H. Kulkarni, Surf. Coat Technol., 158 (2002) 658.
7. M. S. Shah, M. Saleem, R. Ahmad, M. Zakaullah, A. Qayyum and G. Murtaza, J. Mater. Process Technol., 199 (2008) 363.
8. Z. Jianxin, H. Jining, D. Yanchun, L. Xiangzhi and Y. Dianran, J. Mater. Process Technol., 197 (2008) 31.
9. Z. Y. Fan and N. Newman, Appl. Phys. Lett., 73 (1998) 456.
10. S. V. Bagul, S. D. Chavhan and S. Ramphal, J. Phys. & Chem. Solids, 68 (2007) 1623.
11. M. U. Kamachi, H. S. Khatak, R. Baldev and M. Uhlemann, Mat. Manufact. Process, 19 (1) (2004) 61.
12. A. Alsaran and A. Çelik, Mater. Charact., 47 (2001) 207.
13. M Karakan, A Alsaran and A Çelik, Mater. Charact., 49 (2003) 241.
14. T. Fitz and W. Moller, J. Appl. Phys., 92 (11) (2002) 6862.
15. M. Moradshahi, T. Tavakoli, S. Amiri and S. Shayeganmchr, Surf. Coat. Technol., 201 (2006) 567.

16. F. A. Haas, A. Goodyear and N. S. J. Braithwaite, Plasma Sources Sci. Technol., 7 (1998) 471.
17. F. A. Haas and N. S. J. Braithwaite, Appl. Phys. Lett., 74 (1999) 338.
18. H. Shindo, T. Urayama, T. Fujii, Y. Horiike and S. Fujii, Jpn. J. Appl. Phys., 38 (1999) L1066.
19. M. Nisha, K. J. Saji, R. S. Ajimsha, N. V. Joshy and M. K. Jayaraj, J. Appl. Phys., 99 (2006) 033304-1.
20. A. Qayyum, M. Ikram, M. Zakaullah, A. Waheed, G. Murtaza, R. Ahmad, A. Majeed, N. A. D. Khattak, K. Mansoor and K. A. Chaudhry, Int. J. Mod. Phys., B 17 (2003) 1.
21. M. J. Druyvesteyn, Z. Phys., 64 (1930) 781.
22. S. Miyamoto, F. Kanayama, T. Mune and H. Horiike, Nucl. Fusion, 46 (2006) S313.
23. H. Singh and D. B. Graves, J. Appl. Phys., 87(9) (2000) 4098.
24. M. M. Turner, R. A. Doyle and M. B. Hopkins, Appl. Phys. Lett., 62 (1993) 3247.
25. A. Grill, Cold Plasma in Materials Fabrication, IEEE Press, New York, (1993).
26. H. X. Ming, N. Baker, B. A. Kehler, K. C. Walter, M. Nastasi and Y. Nakamura, J. Vac. Sci. Technol., A 18 (1) (2002) 30.
27. E. Badawi, M. A. Abdel-Rahman, S. A. Mahmoud and A. A. Ramadan, Turk. J. Phys., 24 (2000) 543.
28. S. Ohira, K. Hiei and M. Iwaki, Nucl. Instrum. Method Phys. Res., B 32 (1988) 66.
29. L. Wang, S. Ji and J. Sun, Surf. Coat. Technol., 200 (2006) 5067.
30. R. S. Rawat, P. Arun, A. G. Vedeshwar, P. Lee and S. Lee, J. Appl. Phys., 95 (2004) 7725.
31. S. J. Ji, L. Wang, J. C. Sun and Z. K. Hei, Surf. Coat. Technol., 195 (2005) 81.
32. U. Figueroa, O. Salas and J. Oseguera, Thin Solid Films, 469 (2004) 295.
33. T. Telbizova, S. Parascandola, F. Prokert, N. P. Barradas, E. Richter and W. Moller, Surf. Coat. Technol., 142 (2001) 1028.

**34.** **S. Gredelj, A. R. Gerson, S. Kumar and G. P. Cavallaro, Appl. Surf. Sci., 199 (2002) 183.**

**35.** **P. Tyagi and A. G. Vedeshwar, Phys. Rev., B 66 (2002) 075422-1.**

**36.** **M. W. Thompson, Defects and Radiation Damage in Metals, University Press, Cambrigde, (1969).**

**37.** **G. Knuyt, W. Lauwerens and L. M. Stals, Thin Solid Films, 370 (2000) 232.**

**38.** **Z. D. Xiang and P. K. Datta, Scripta Materialia, 55 (2006) 1151.**

**39.** **S. Gredelj, A. R. Gerson, S. Kumar and G. P. Cavallaro, Appl. Surf. Sci., 174 (2001) 240.**

**40.** **M. Quast, P. Mayr and H. –R. Stock, Surf. Coat. Technol., 120/121 (1999) 244.**

**41.** **A. Zhecheva, S. Wei, S. Malinov and Adrian Long, Surf. Coat. Technol., 200 (2005) 2192.**

PK ISSN 0022- 2941; CODEN JNSMAC
Vol. 49, No.1 & 2 (April & October 2009) PP 19-25

# JORDAN ZERO-PRODUCT PRESERVING ADDITIVE MAPS ON NEST ALGEBRAS

**A. MAJEED AND J. Li**

Department of Mathematics, East China University of Science and Technology, Shanghai 200237, China
E-mail Addresses: asiamajeed@hotmail.com

**(Received: April 19, 2010)**

**ABSTRACT:** Let AlgN and AlgM be nest algebras associated with the nests N and M on Hilbert spaces. Let $\phi$: AlgN $\rightarrow$ AlgM be an additive bijective map. $\phi$ preserves Jordan zero-products in both directions, that is $\phi$(A)$\phi$(B)+$\phi$(B)$\phi$(A)=0 $\Leftrightarrow$ AB+BA = 0. In this paper we show that, under some mild conditions $\phi$ is a Jordan homomorphism multiplied by a central element.

**Keywords:** Nest algebras, Jordan zeroproducts, Jordan homomorphism.

## 1. INTRODUCTION

Let H denotes an infinite-dimensional Hilbert spaces. Let B(H) and F(H) denote the set of all bounded linear operators on H and the set of all finite rank operators on H respectively. We use the symbols x $\otimes$ y and I to denote the rank one operator <˙,˙>x and the unit operator on H, respectively. If we denote by N a complete nest on H, then the nest algebra algN is the set of all operators which leave every member of N invariant. The algebra algN is a Banach algebra. If $N_1 \in$ N, we write $N_{1-}$ for $\vee$\{M$\in$N: M$\subset N_1$\}. We say that N is a continuous nest if $N_{1-} = N_1$ for any $N_1 \in$ N. If N is a closed subspace in H, we write P(N) for the orthogonal projection operator from H onto N.

For notation, we use lower case letters to represent elements of rings and algebras in the abstract setting and capital letters to represent elements of sub algebras of Hilbert space operators.

**$\phi$ is said to preserve Jordan zero-product in both direction if $\phi$(A)$\phi$(B) + $\phi$(B)$\phi$(A) = 0 $\Leftrightarrow$ AB + BA= 0.**

**In section 2, we omit the assumption of "in both direction", and use a different approach to show that, for real or complex Hilbert space H, every Jordan zero-product preserving additive bijection on nest algebra has either the form $\phi$(A) = cUA$U^{-1}$ for all A $\in$algN or the form $\phi$(A) = cUA*$U^{-1}$ for all A $\in$algN, where c is a non-zero scalar, U is a bounded invertible linear or conjugate, linear operator and A*$\in$ N is the adjoint of A.**

**Let $\phi$ be a map between two rings. We say that $\phi$ is a zero-product preserving if $\phi$(A)$\phi$(B) = 0 whenever AB = 0.**

**Definition 1.1: Let $\phi$ be a map between two rings. We say that $\phi$ is Jordan zero-product preserving if**
**$\phi$(A)$\phi$(B)+$\phi$(B)$\phi$(A)=0 whenever AB + BA = 0.**

**Definition 1.2: Let A, B be Jordan rings. An additive map $\phi$ : A$\rightarrow$B is said to be a Jordan ring homomorphism if $\phi$(TS+ST) =$\phi$(T)$\phi$(S) +$\phi$ (S)$\phi$(T) for all elements T, S in A.**

**Definition 1.3: Let A, B be Jordan rings. An additive map $\phi$ : A$\rightarrow$B is said to be a Jordan ring homomorphism if $\phi$($T^2$) =$\phi$ $(T)^2$ for all T in A.**

## 2. MAIN RESULTS

**Theorem 1: Let H and K be (real or complex) infinite-dimensional Hilbert spaces. Let $N_1$ and $N_2$ be nests in B(H) and B(K) respectively. Let $\phi$ : alg $N_1 \rightarrow$ alg $N_2$ be a Jordan zero-product preserving strongly continuous additive bijection. Then there exists a non-zero scalar c and an invertible**

**bounded linear or conjugate-linear operator U:H $\to$ K such that either $\phi$(A) = cUA$U^{-1}$ for all A $\in$ alg $N_1$ or $\phi$(A) = cUA* $U^{-1}$ for all A $\in$ alg $N_1$ (in real case U is linear).**

**Proof: Let P $\in$ alg $N_1$ with $P^2$ = P. Since P(I-P)+(I-P)P = 0. We have**

**$\phi$(P)$\phi$(I-P) + $\phi$(I-P)$\phi$(P) = 0, and consequently,**

**$\phi$(I)$\phi$(P) + $\phi$(P)$\phi$(I) = 2$\phi(P)^2$.**

**Thus we have**

**$\phi\left(P\right)^2\phi(I) + \phi(P)\phi(I)\phi(P) = 2\phi(P)^3$**

**and**

**$\phi(I)\phi\left(P\right)^2 + \phi(P)\phi(I)\phi(P) = 2\phi(P)^3$.**

**Thus these together imply that $\phi(I)\phi\left(P\right)^2 = \phi\left(P\right)^2\phi(I)$. ~~~~~ (*)**

**Similarly, it follows from**

**$\phi\left(I\right)^2\phi(P) + \phi(I)\phi(P)\phi(I) = 2\phi(I)\phi\left(P\right)^2$**

**and**

**$\phi(P)\phi\left(I\right)^2 + \phi(I)\phi(P)\phi(I) = 2\phi\left(P\right)^2\phi(I)$**

**that is**

**$\phi(P)\phi\left(I\right)^2 = \phi\left(I\right)^2\phi(P)$.**

**Every rank one operator in nest algebra is denoted as a linear combination of at most four idempotents by [1] and every finite rank operator in nest algebra may be represented as a sum of rank one operators by [1]. Hence we have**

**$\phi(F)\phi\left(I\right)^2 = \phi\left(I\right)^2\phi(F)$, ~~ for ~~all~~ F~ $\in$ F(H) $\cap$ algN.**

**Since $\phi$ is a strongly operator topology continuous mapping and $\overline{\text{algN} \cap F(H)}^{sot}$ = algN by [1].**

**Hence we have $\phi(A)\phi(I)^2 = \phi(I)^2\phi(A)$ holds for every $A \in \text{alg}\,N_1$. Therefore, by the bijectivity of $\phi$, $\phi(I)^2 = \lambda I$ for some scalar $\lambda$. Let T, S $\in$ alg $N_1$ with ST = 0. For any idempotent P, it follows from TP(I-P)S + (I-P)STP = 0 that $\phi(TP)\phi((I-P)S) + \phi((I-P)S)\phi(TP) = 0$.**

**Thus $\phi(TP)\phi(S) + \phi(S)\phi(TP) = \phi(TP)\phi(PS) + \phi(PS)\phi(TP)$ (1)**

**holds for every idempotent P. On the other hand, T(I-P)PS + PST(I-P) = 0 implies that $\phi(T(I-P))\phi(PS) + \phi(PS)\phi(T(I-P)) = 0$, and hence,**

**$\phi(T)\phi(PS) + \phi(PS)\phi(T) = \phi(TP)\phi(PS) + \phi(PS)\phi(TP)$ (2)**

**for every idempotent P. Combining (1) and (2), we get**

**$\phi(TP)\phi(S) + \phi(S)\phi(TP) = \phi(T)\phi(PS) + \phi(PS)\phi(T)$**

**for every idempotent P. Hence for every A $\in$ alg $N_1$,**

**$\phi(TA)\phi(S) + \phi(S)\phi(TA) = \phi(T)\phi(AS) + \phi(AS)\phi(T)$. (3)**

**Take T = Q and S = I-Q for some Q $\in$ alg $N_1$ with $Q^2$ = Q. Then ST = 0 and from (3), one gets $\phi(QA)\phi(I-Q) + \phi(I-Q)\phi(QA) = \phi(Q)\phi(A(I-Q)) + \phi(A(I-Q))\phi(Q)$. Thus we see that $\phi(QA)\phi(I) + \phi(I)\phi(QA) - \phi(Q)\phi(A) - \phi(A)\phi(Q)$**
**$= \phi(QA)\phi(Q) + \phi(Q)\phi(QA) - \phi(Q)\phi(AQ) - \phi(AQ)\phi(Q)$.**

**On the other hand, taking T = I-Q and S = Q, we obtain from (3)**
**$\phi(I)\phi(AQ) + \phi(AQ)\phi(I) - \phi(A)\phi(Q) - \phi(Q)\phi(A) = \phi(Q)\phi(AQ) + \phi(AQ)\phi(Q) - \phi(QA)\phi(Q) - \phi(Q)\phi(QA)$.**

**Hence**

**$\phi(QA + AQ)\phi(I) + \phi(I)\phi(QA + AQ) = 2(\phi(Q)\phi(A) + \phi(A)\phi(Q))$**

**holds for every idempotent Q. This further implies that**

**$\phi(AB + BA)\phi(I) + \phi(I)\phi(AB+BA) = 2(\phi(A)\phi(B) + \phi(B)\phi(A))$ (4)**

**holds for every $B \in \text{alg}\,N_1$. Multiplying (4) from left and right by $\phi(I)$ respectively, we see that**

$\phi(I)^2 \phi(AB + BA) + \phi(I) \phi(AB + BA)\phi(I) = 2\phi(I)(\phi(A)\phi(B) + \phi(B)\phi(A))$

**And**

$\phi(I) \phi(AB + BA) \phi(I) + \phi(AB + BA) \phi(I)^2 = 2(\phi(A) \phi(B) + \phi(B) \phi(A)) \phi(I).$

**These two equations, together with the fact that** $\phi(I)^2 = \lambda I$**, entail that**

$$\phi(I)(\phi(A)\phi(B) + \phi(B)\phi(A)) =(\phi(A)\phi(B) + \phi(B)\phi(A))\phi(I). \quad (5)$$

**Let A = B in (4) and (5); then**

$$\phi(I)\phi(A^2) + \phi(A^2)\phi(I) = 2\phi(A)^2, \quad (6)$$

$$\phi(I)\phi(A)^2 = \phi(A)^2\phi(I). \quad (7)$$

**By the bijectivity of** $\phi$**, Eq. (7) implies that** $\phi(I)$ **commutes with all idempotent operators and hence there must exist a scalar** $\mu$ **such that** $\phi(I) = \mu I$**. While Eq. (6) tells that** $\mu \neq 0$**. Let c =** $\frac{1}{\mu}$ **and** $\varphi(.) = c\,\phi(.)$**, then** $\varphi$ **:alg** $N_1 \to$ **alg** $N_2$ **is strongly continuous additive bijection preserving Jordan zero-products and** $\varphi(I) = I$**. Moreover, for every A** $\in$ **alg** $N_1$, $\varphi(A^2) = \varphi(A)^2$**, which implies that** $\varphi$ **is a Jordan ring homomorphism.**

**Now we consider the finite dimensional case. It is clear that every nest algebra on finite dimensional spaces is isomorphic to an upper triangular block matrix algebras. So, without loss of the generality we may discuss the question for upper triangular block matrix algebras. Let** $M_n = M_n$**(F) be the matrix algebra over field F. Let T =T**$(n_1, n_2, \ldots\ldots, n_k) \subset M_n$ **be upper triangular block matrix sub algebra, i.e.,** $(n_1, n_2, \ldots\ldots, n_k)$ **= n,T = {A =** $(A_{ij})_{kxk} \mid A_{ij} \in M_{n_i,n_j}$ **and** $A_{ij}$ **=0 if i>j}.**

**Corollary: Let F be a real/complex field, and m and n be positive integers greater than 1. Let T = T**$(n_1, n_2, \ldots\ldots, n_k) \subset M_n$**(F) and T = T**$_1$**(**$m_1, m_2, \ldots, m_r$**)**

**$\subseteq$ $M_m$(F) be upper triangular block matrix algebras, and let $\phi: T_1 \to T$ be a Jordan zero-product preserving additive bijection. If $(n_1, n_2, \ldots\ldots, n_k)$ = $(m_1, m_2, \ldots\ldots, m_r)$ then there exists a nonzero scalar c and an invertible matrix U $\in$ T s.t either $\phi$(A) = cUA$U^{-1}$ for all A $\in$ T or $\phi$(A) = cU$A^{tr}$ $U^{-1}$ for all A $\in$ T.**

## 3. INFINITE MULTIPLICITY

**DEFINITION 3.1: Let H be a complex separable Hilbert space. Let W be a weakly closed sub algebra of B(H). If K is also a complex separable Hilbert space, then the tensor product W$\otimes$B(K) is defined as the weak operator closure of the span of all elementary tensors A$\otimes$B acting on H$\otimes$K , where A $\in$W and B $\in$B(H). A weakly closed sub algebra W of B(H) is said to be infinite multiplicity if W$\otimes$B(K) is isomorphic to W.**
**In [2], L. Marcoux, A. Sourour proved the following lemma:**

**Lemma 3.1: Let W be a weakly closed, unital algebra of B(H) of infinite multiplicity. Then every A$\in$W is a sum of eight idempotents in W.**

**Theorem: Let W be as in Lemma 3.1. If H and K are complex separable Hilbert spaces and let $W_1$ be a weakly closed, unital algebra of B(H) of infinite multiplicity and $W_2$ be a weakly closed, unital algebra of B(K) of infinite multiplicity. Suppose $\phi: W_1 \to W_2$ is a Jordan zero-product preserving additive bijection. Then there exists a non-zero scalar c and an invertible linear or conjugate linear operator U:H $\to$K such that either $\phi$(A)=cUA$U^{-1}$for all A$\in$ $W_1$ or $\phi$(A)=cUA* $U^{-1}$for all A$\in$ $W_1$ (in real case U is linear).**

**Proof: Let P$\in$ $W_1$ with $P^2$=P By (*), we have that for any idempotent P$\in$ $W_1$,**

$\phi$ **(P)** $\phi\left(\mathrm{I}\right)^2$ **=** $\phi\left(\mathrm{I}\right)^2\phi$ **(P).**

**By Lemma 3.1, we have that every A $\in$ W is a sum of eight idempotents in W . Hence we have**

$\phi$ **(A)** $\phi\left(\mathrm{I}\right)^2$ **=** $\phi\left(\mathrm{I}\right)^2\phi$ **(A). (8)**

**holds for every A $\in$ $\mathrm{W}_1$.Therefore, by the bijectivity of $\phi$ , $\phi\left(\mathrm{I}\right)^2$ = $\lambda$ I for some scalar $\lambda$ .**

**Similarly we can easily get,**

$\phi$ **(I)** $\phi$ **(** $\mathrm{A}^2$ **)+** $\phi$ **(** $\mathrm{A}^2$ **)** $\phi$ **(I) =2** $\phi$ $(\mathrm{A})^2$ **, (9)**

$\phi$ **(I)** $\phi$ $(\mathrm{A})^2$ **=** $\phi$ $(\mathrm{A})^2$ $\phi$ **(I). (10)**

**by using Eqs. (9) and (10).**

**By the bijectivity of $\phi$, Eq. (10) implies that $\phi$(I) commutes with all idempotent operators and hence there must exist a scalar $\mu$ such that $\phi$(I) = $\mu$ I. While Eq. (9) tells that $\mu \neq 0$. Let c= $\frac{1}{\mu}$ and $\varphi$(.) = c $\phi$ (.), then $\varphi$ : $\mathrm{W}_1$ $\rightarrow \mathrm{W}_2$ is an additive bijection preserving Jordan zero-products and $\varphi$(I) = I. Moreover, for every A $\in \mathrm{W}_1$, $\varphi$( $\mathrm{A}^2$ ) = $\varphi$ $(\mathrm{A})^2$, which implies that $\varphi$ is a Jordan ring homomorphism.**

## REFERENCES


1. **J. A. Erdos, J. Lon. Math. Soc., 43 (1968) 391.**
2. **L. Marcoux and A. Sourour, J. Lon. Math. Soc., 65 (2002) 493.**
3. **J. Hou and M. Jiao, Linear Algebra Appl., 422 (2007) 721.**
4. **L. Zhao and J. Hou, J. Math. Anal. Appl., 314 (2006) 689.**

PK ISSN 0022- 2941; CODEN JNSMAC
Vol. 49, No.1 & 2 (April & October 2009) PP 27-31

# INVESTIGATION BY SYNCHROTRON RADIATION OF InGaAs LASING STRUCTURES GROWN ON SiGe/Si PSEUDOSUBSTRATES

A. R. KHAN, K. MUNDBOTH, J. STANGL, M. MEDUŇA, E. WINTERSBERGER AND G. BAUER

Institute for Semiconductor and Solid State Physics, University of Linz, A-4040 Linz, Austria
Corresponding Author: aaliya.rehman@gmail.com

(Received: September 23, 2010)

**ABSTRACT:** The growth of highly strained Quantum wells (QWs) on GaAs substrates are facilitated by the initial growth of a linearly graded InGaAs buffer. High-resolution X-ray diffractometry can supply overall information about the quality of the samples while X-ray topography provides both direct evidence of the absence or presence of single defects and visualization of their distribution. We present here a summary of studies performed on these InGaAs/AlGaAs QWs.

**Keywords:** Synchrotron radiation; pseudosubstrates.

## 1. INTRODUCTION

Intersubband transitions have been used for applications such as photodetectors, modulators, and nonlinear optics [1-3]. By using InGaAs and AlGaAs for the well and barrier materials, respectively, quantum wells (QWs) can have large conduction band offset, and thus, large intersubband transition energies [4,5]. A series of two samples including an InGaAs layer structure was investigated by X-ray diffraction experiment at University of Linz using a rotating anode source with a conventional laboratory setup and position sensitive detector and at synchrotron source HASYLAB at beam line D4 in Hamburg. A schematic sketch of the sample structure and the nominal structural parameters are shown in Fig.1.

The difference between the samples Ge101 and Ge102 was in the used pseudosubstrate. Sample Ge101 was grown on constant composition Ge/Si(001) pseudosubstrate and Ge102 on constant composition Ge/graded SiGe/Si pseudosubstrate with 6° mis-orientation.

| 207 nm GaAs |
| --- |
| 2000 nmAl0,3GaAs |
| 167 nm GaAs |
| 8 nm InGaAs |
| 167 nm GaAs |
| 2000 nm Al0,3GaAs |
| 1035nm GaAs |
| 374nm GaAs HT |
| 60nm GaAs BT |
| PS |

**Fig.1: Schematic sketch of sample structure of samples Ge101 (constant composition buffer) and Ge102 (graded SiGe buffer).**

**In order to study the relaxation and strain properties of Ge, GaAs and InGaAs layers, a symmetrical (004) and asymmetrical (224) diffraction reciprocal space maps have been measured in two perpendicular azimuths [6]. The example of XRD reciprocal space maps around the (004) and (224) diffraction for sample Ge101 is shown in Fig.2.**

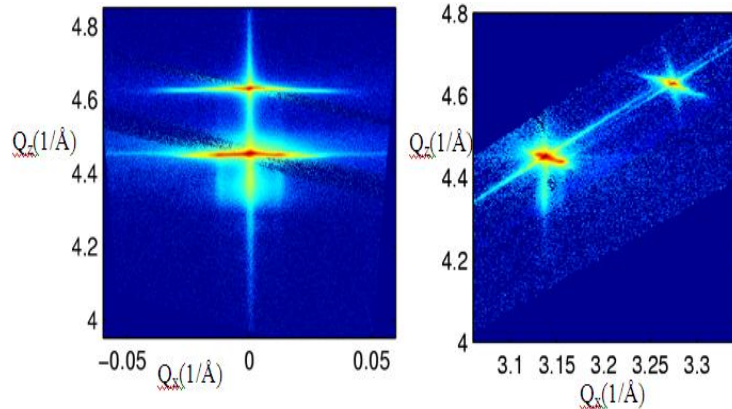


**Fig.2: Symmetrical 004 (left panel) and asymmetrical 224 (right panel) diffraction reciprocal space maps of the sample Ge101 under two different azimuths, aligned to Ge buffer peak.**

## 2. RESULTS AND DISCUSSION

**From the asymmetrical (224) reciprocal space map, we can clearly see that the InGaAs layer is grown pseudomorphically with respect to GaAs/Ge buffer. The detailed analysis of the position of $In_xGa_{1-x}As$ peak at $Q_z$=(4.380 ± 0.005) 1/Å gives an average lattice parameter of $In_xGa_{1-x}As$ layer of $a_{||}$ = (5.738 ± 0.007) Å. Using a dependence of In composition in $In_xGa_{1-x}As$ alloy on the lattice parameter [8], we get a corresponding In content of x=(0.26 ± 0.04).**

**From the symmetrical (004) reciprocal space map, it is also evident that the InGaAs layer, responsible for lasing emission, exhibits also a lateral periodicity presented by two satellite maxima in distance of (0.0115 ± 0.0005) 1/Å from 0$^{th}$ InGaAs peak in $Q_x$ direction. After analysis, we find out that such position of the maxima correspond to the lateral period of about (546 ± 24) Å. This could correspond to the formed island at the InGaAs layer, Fig 3.**

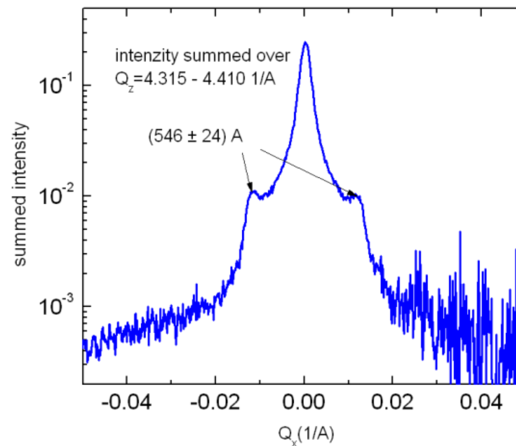


**Fig.3: Intensity integrated through lateral maxima over $Q_z$ direction over interval $Q_z$ = (4.315 - 4.410) 1/Å.**

**In order to investigate the strain properties of the GaAs and InGaAs layer more carefully, we have measured also the symmetrical (002) diffraction, see Fig. 4, which is forbidden for Si and Ge but not for the GaAs. Since Ge and GaAs have almost the same lattice parameter, close the (004)**

**reciprocal lattice point; the GaAs diffraction signal is disturbed by Ge diffraction signal. In (002) we detect only the signal from GaAs and InGaAs. In the (002) reciprocal space map recorded at HASYLAB beamline D4 in Hamburg, we clearly see the diffraction peak from pure GaAs layers, from InGaAs layer and also a peak at position Qz = 2.313 1/Å most probably corresponding to the layer with lattice parameter $a_{perp}$= (5.433 ± 0.010) 1/Å.**

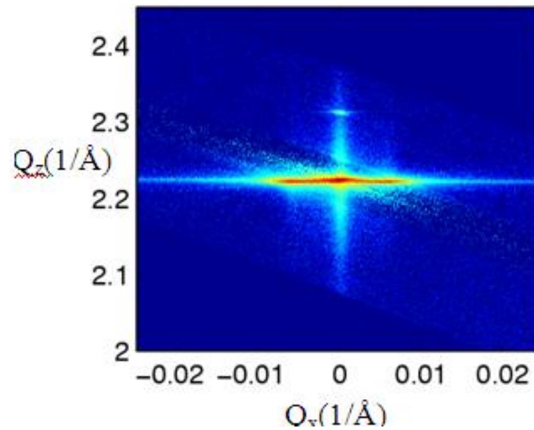


**Fig.4: Symmetrical 002 diffraction reciprocal space maps of the sample Ge101.**

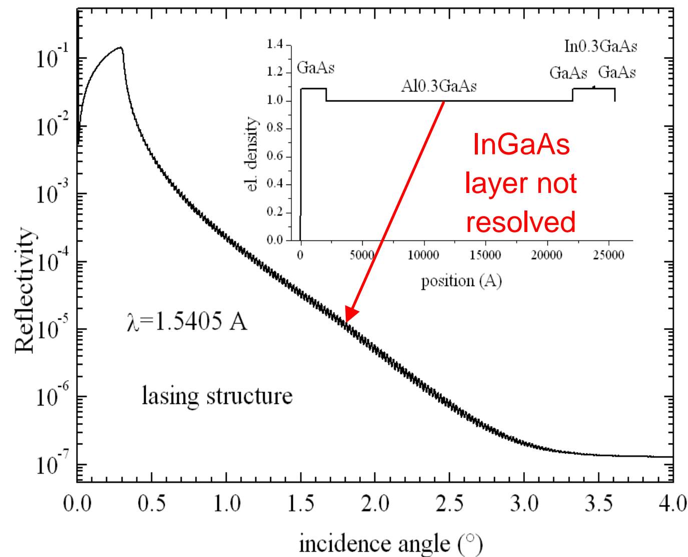


**Fig. 5: Specular reflectivity simulation on the sample structure.**

From theoretical simulations it follows, Fig.5, that it is not possible to perform a specular reflectivity measurement in order to obtain information about the interface morphology at InGaAs layer interface and to detect the thin InGaAs layer in reflectivity at all, since the penetration depth is not large enough for grazing incidence angles and usual wavelengths. The InGaAs layer is situated too deep in the structure for XRR investigation [7,8].

## REFERENCES


1. E. Rosencher, B. Vinter and B. Levine, *Intersubband transitions in quantum wells,* Plenum, New York, 1992.
2. C. G. Bethea, B. F. Levine, V. O. Shen, R. R. Abbott, and S. J. Hsieh, IEEE Electron. Devices, 38 (1991) 1118.
3. M. M. Fejer, S. J. B. Yoo, R. L. Byer, A. Harwit and J. S. Harris, Phys. Rev. Lett., 62 (1989) 1041.
4. S. M. Lord, B. Pezeshki and J. S. Harris, Jr., Electron. Lett., 28 (1992) 1193.
5. H. C. Chui, S. M. Lord, E. Martinet, M. M. Fejer and J. S. Harris, Jr., Appl. Phys. Lett., 63 (1993) 364.
6. U. Pietsch, V. Holý and T Baumbach, *High-Resolution X-Ray Scattering*, Springer Verlag, Berlin 2004.
7. A. Authier, *Dynamical Theory of X-Ray Diffraction*, Oxford University Press, Oxford 2001.
8. A. C. Ferrari MRS Symposium Proceedings, 675 (2001) p W11.5.

PK ISSN 0022- 2941; CODEN JNSMAC
Vol. 49, No.1 & 2 (April & October 2009) PP 33-47

# COMMON FIXED POINT THEOREMS IN FUZZY METRIC SPACES FOR SEMI-COMPATIBLE MAPPINGS

***M. A. KHAN, *SUMITRA AND ** R. CHUGH**

*Department of Mathematics, Eritrea Institute of Technology, Asmara, Eritrea (N. E. Africa)
**Maharishi Dayanand University, Rohtak-Haryana, India
E-mail Addresses: alam3333@gmail.com

**(Received: February 08, 2009)**

**ABSTRACT:** The intent of this paper is to establish some common fixed point theorems through semi-compatibility for quadruple self maps, two of which are semi-compatible and remaining two are weak compatible. In our theorems the completeness of the space X and the continuity of maps is replaced with a set of four alternative conditions for functions satisfying implicit relations. These theorems extend and improve the results of B. Singh and S. Jain [1-4] and Mishra et. al. [5].

2000 AMS Classification: 47H10, 54H25.
**Keywords**: Compatible maps, Semi-compatible maps, weak compatible maps, fixed points and fuzzy metric space.

## 1. INTRODUCTION

Cho et. al. [6] introduced the notion of semi-compatible maps in d-topological spaces. Various authors like Saliga [7], Sharma et al. [8] and Popa [9] proved some interesting fixed point results using implicit real functions and semi-compatibility in d-complete topological spaces.

Recently B. Singh and S. Jain [1,3,4] introduced the concept of semi-compatibility in fuzzy metric spaces, D-metric spaces, 2-metric spaces and proved fixed point results using implicit relations in these spaces.

The main objective of this paper is to obtain some fixed point theorems in the setting of fuzzy metric spaces using weak compatibility, semi-compatibility and an implicit relation without considering the completeness of the space X and continuity of maps. The relationship between compatible, weak compatible and semi-compatible maps has also been established. We first give some preliminaries and definitions using [10,11].

## 2. PRELIMINARIES

**DEFINITION 2.1: A binary operation** $*:[0,1]\times[0,1]\rightarrow[0,1]$ **is continuous** $t-norm$ **if** $*$ **satisfies the following conditions:**

**(i)** $*$ **is commutative and associative**

**(ii)** $*$ **is continuous**

**(iii)** $a*1=a \ for \ all \ a\in[0,1]$

**(iv)** $a*b\leq c*d \ whenever \ a\leq c \ and \ b\leq d \ , a,b,c,d\in[0,1]$.

**DEFINITION 2.2: The triplet *(X, M, *)* is said to be a fuzzy metric space if X is an arbitrary set,** $*$ **is a continuous** $t-norm$ **and M is a fuzzy set on** $X^2\times[0,\infty)$ **satisfying the following;**

**(FM-1)** $M(x,y,t)>0$

**(FM-2)** $M(x,y,t)=1 \ if \ and \ only \ if \ x=y.$

**(FM-3)** $M(x,y,t)=M(y,x,t)$

**(FM-4)** $M(x,y,t)*M(y,z,s)\leq M(x,z,t+s)$

**(FM-5)** $M(x,y,\bullet):[0,\infty)\rightarrow[0,1]$ **is left continuous for all** $x,y,z\in X$ **and** $s,t>0$.

**Note that *M (x, y, t)* can be thought of as the degree of nearness between x and y with respect to *t*.**

**Example 1([12]): (Induced fuzzy metric space) Let (X, d) be a metric space and a * *b* = *a b* for all *a, b*** $\in$ **[0, 1] and let** $M_d$ **be fuzzy set on** $X^2\times[0,\infty)$ **defined as follows;**

$$M_d(x,y,t)=\frac{t}{t+d(x,y)}.$$

**Then** $(X, M_d, *)$ **is a fuzzy metric space. We call this fuzzy metric induced by a metric *d*.**

**Example 2 ([12]): Let *X = N. Define a * b = max {0, a + b – 1} for all a, b* ∈ [0, 1] and let, M be a fuzzy set on $X^2 \times [0,\infty)$ as follows;**

$$M(x,y,t)=\begin{cases}\dfrac{x}{y} & if \quad x\le y\\ \dfrac{y}{x} & if \quad y\le x\end{cases} \quad for\ all\ x,y\in X.$$

**Then *(X, M, *)* is a fuzzy metric space.**

**Note that in the above example, there exists no metric d on X, satisfying**

$$M(x,y,t)=\frac{t}{t+d(x,y)},$$

**Where *(X, M, *) is* defined in above example. Also note that the above function M is not a fuzzy metric with the $t-norm$ defined as *a * b* = min *{a, b}*.**

**DEFINITION 2.3: Let *(X, M, *)* be a fuzzy metric space. Then**

**(a) A sequence $\{x_n\}$ in X is said to be convergent to x if for each $\varepsilon > 0$ and each $t > 0$, there exists $n_0\in N$ such that** $M(x_n,x,t)>1-\varepsilon \ for\ all\ n\ge n_0$

**(b) The sequence $\{x_n\}$ in X is said to be Cauchy if for each $\varepsilon>0$ and for each $t > 0$, there exists $n_0\in N$** such that

$$M(x_n,x_m,t)>1-\varepsilon \ for\ all\ n,m\ge n_0.$$

**(c) A fuzzy metric space in which every Cauchy sequence is convergent is said to be complete.**

**PREPOSITION 1 ([12]): In a fuzzy metric space *(X, M, *)* if $a * a \ge a$ for all $a \in [0, 1]$, $a * b = min\ \{a, b\}$ for all $a, b \in [0, 1]$.**

**Let *(X, M, *)* be a fuzzy metric space with the condition;**

$\lim_{t\to\infty} M(x,y,t)=1$ **for all x , y in X. (FM-6)**

**Lemma 1 ([13]): Let $\{y_n\}$ be a sequence in a fuzzy metric space *(X, M, *)* with the condition (FM-6). If there exists a $k \in (0, 1)$ such that $M(y_n, y_{n+1}, kt) \ge M(y_{n-1}, y_n, t)$ for all $t > 0$ and $n \in N$, then $\{y_n\}$ is a Cauchy sequence in *X*.**

**DEFINITION 2.4: Two self mappings A and S of a fuzzy metric space *(X, M, *)* are called compatible if**

$$\lim_n M\left(ASx_n, SAx_n, t\right) = 1,$$

**Where *{$x_n$}* is a sequence in X such that** $\lim_n Ax_n = \lim_n Sx_n = x,$ **for some x in X.**

**DEFINITION 2.5: Two self mappings A and S of a fuzzy metric space *(X, M, *)* are called weakly compatible if they commute at their coincidence points *i.e.*, if**

***A x = S x* then *S A x = A S x*.**

**DEFINITION 2.6: Two self mappings** $A, B : X \to X$ **are said to be semi-compatible if**

$$\lim_n M\left(ABx_n, Bx, t\right) = 1 \text{ , for all } t > 0$$

**whenever *{$x_n$}* is a sequence in X such that**

$$\lim_n Ax_n = \lim_n Bx_n = x, \text{ for some } x \in X.$$

**It follows that if *(A, B)* is semi-compatible and *A y = B y* then *A B y = B A y.* Thus semi-compatibility implies weak compatibility but converse is not true.**

**Remark 1: Compatibility implies weak compatibility but the converse is not true as shown in the following example:**

**Example 3: Let *(X, M, *)* be a fuzzy metric space where *X = [0, 2]* and** $t-norm$ **be defined as *a * b* = min *{a, b}* where *a, b* ∈ *[0, 1]* and**

$$M\left(x, y, t\right) = \frac{t}{t+|x-y|} \; for \; all \; x, y \in X, t > 0.$$

**Define self maps** $A, S : X \to X$ **as**

$$A\left(x\right) = \begin{cases} 2-x, & 0 \le x < 1 \\ 2 & 1 \le x \le 2 \end{cases}, \; S\left(x\right) = \begin{cases} x, & 0 \le x < 1 \\ 2 & 1 \le x \le 2 \end{cases}.$$

**Consider the sequence** $\langle x_n \rangle = 1 - \frac{1}{n}$ **, then** $A\left(x_n\right) = 2 - \left(1 - \frac{1}{n}\right) = 1 + \frac{1}{n}.$

$$S(x_n) = 1 - \frac{1}{n}, \; ASx_n = A\left(1 - \frac{1}{n}\right) = 2 - \left(1 - \frac{1}{n}\right) = 1 + \frac{1}{n}.$$

$$SAx_n = S\left(1 + \frac{1}{n}\right) = 2.$$

**Thus,** $\lim_n M(ASx_n, SAx_n, t) = \lim_n M\left(1 + \frac{1}{n}, 2, t\right) \neq 1 \; for \; all \; t > 0.$

**This implies that (A, S) is not compatible. But the set of coincidence points of A and S is [1, 2].**

**Now, for any** $x \in [1,2], \; Ax = Sx = 2 \; and \; ASx = A(2) = 2 = SAx.$ **Thus, A and S are weak compatible but not compatible.**

**Also**

$$Ax_n, Sx_n \to 1 \; and \; \lim_n M(ASx_n, S1, t) = \lim_n M\left(1 + \frac{1}{n}, 2, t\right) \neq 1$$

**This implies that (A, S) is not semi-compatible. But *(A, S)* is weak compatible and thus weak compatibility not implies the semi-compatibility.**

**Again**

$$\lim_n M(SAx_n, A1, t) = \lim_n M(2, 2, t) = 1$$

**Which implies that *(S, A)* is semi-compatible but *(A, S)* is not semi-compatible. Thus, semi-compatibility of *(S, A)* does not imply the semi-compatibility of *(A, S)*. Now, we show that compatibility does not imply semi-compatibility.**

**Example 4: Let X= [0, 1] with t-norm**

$$\Delta(a,b) = \min\{a,b\}, a, b \in [0,1].$$

**Set**

$$M(x, y, t) = \frac{t}{t + |x - y|} \; for \; all \; x, y \in X \; and \; t > 0.$$

**Then, *(X, M, *)* is fuzzy metric space.**

**Define self mappings $A, B : X \to X$ as**

$$A(x) = x \ , \ \ B(x) = \begin{cases} x & 0 \le x < \frac{1}{2} \\ 1 & x \ge \frac{1}{2} \end{cases}.$$

**Taking**

$$\langle x_n \rangle = \frac{1}{2} - \frac{1}{n}.$$

**Then**

$$A(x_n) = \frac{1}{2} - \frac{1}{n} \to \frac{1}{2} \ , \ B(x_n) = \frac{1}{2} - \frac{1}{n} \to \frac{1}{2}$$

$$ABx_n = A\left(\frac{1}{2} - \frac{1}{n}\right) = \frac{1}{2} - \frac{1}{n} \ \ and \ \ BAx_n = B\left(\frac{1}{2} - \frac{1}{n}\right) = \frac{1}{2} - \frac{1}{n}.$$

**Thus**

$$\lim_n M\left(ABx_n, BAx_n, t\right) = 1.$$

**Which implies that A and B are compatible.**

**But**

$$\lim_n M\left(ABx_n, B\frac{1}{2}, t\right) = \lim_n M\left(\frac{1}{2} - \frac{1}{n}, 1, t\right) \ne 1.$$

**Which implies that *(A, B)* is not semi-compatible.**

**Class of Implicit Relation: Let $\Phi$ be the set of all continuous functions $\Phi : \left(R^+\right)^5 \to R$, non-decreasing in first argument and satisfying the following conditions;**

**(i)** **For** $u, v \ge 0, \Phi(u,u,v,u,v) \ge 0 \ \ or \ \ \Phi(u,v,u,v,u) \ge 0 \ implies\, u \ge v$.

**(ii)** $\Phi(u,u,1,u,1) \ge 0 \ implies \ \ u = 1$.

**In [1], B. Singh and S. Jain proved the following theorem.**

**Theorem 1: Let *A, B, S* and *T* be self maps on a complete fuzzy metric space *(X, M, *)* satisfying:**

**(i)** $A(X) \subseteq T(X)$, $B(X) \subseteq S(X)$

**(ii) One of *A* or *B* is continuous.**

**(iii) *(A, S)* is semi-compatible and *(B, T)* is weak compatible.**

**(iv) for all** $x, y \in X$ **and** $t > 0$, $M(Ax, By, t) \geq \phi(M(Sx, Ty, t))$ **where** $\phi : [0,1] \to [0,1]$ **is a continuous function such that** $\phi(t) > t$ **for each** $0 < t < 1$**. Then *A, B, S* and *T* have a unique common fixed point.**

**U. Mishra et. al. [5] improved the above theorem in the following form:**

**Theorem 2: Let A, B, S and T be self maps on a complete fuzzy metric space (X, M, *) where** $*$ **is a continuous** $t-norm$ **defined by *a * b* = min *[a, b]* satisfying:**

**(i)** $A(X) \subseteq T(X)$, $B(X) \subseteq S(X)$

**(ii) *(B, T)* is weak compatible.**

**(iii) for all** $x, y \in X$ **and** $t > 0$, $M(Ax, By, t) \geq \phi(M(Sx, Ty, t))$ **where** $\phi : [0,1] \to [0,1]$ **is a continuous function such that** $\phi(1) = 1$, $\phi(0) = 0$ *and* $\phi(a) > a$ **for each *0 < a < 1*. If *(A, S)* is semi-compatible pair of reciprocal continuous maps then, *A, B, S* and *T* have a unique common fixed point.**

**Now, we give generalization of the results of [1] and [17] in the following way.**

## 3. MAIN RESULTS

**Theorem 3: Let *(X, M, *)* be a fuzzy metric space with $a * a \geq a$ for all $a \in [0, 1]$ and the condition (FM-6). Let *A, B, S, T* : $X \to X$ be self maps satisfying**

**(1.1)** $A(X) \subseteq T(X),\ B(X) \subseteq S(X)$

**(1.2) There exists $k \in (0, 1)$ such that**

$$M(Ax, By, kt) \geq M(Sx, Ax, t) * M(Ty, By, t) * M(Sx, Ty, t) * M(Ty, Ax, \alpha t) * M(Sx, By, (2-\alpha)t) \text{ for all } x, y \in X,\ \alpha \in (0,2) \text{ and } t > 0.$$

**(1.3) The pair *(A, S)* is semi-compatible and the pair *(B, T)* is weak compatible.**

**(1.4) One of *A(X), T(X), B(X) or S(X)* is complete**

**(1.5) There exists $F \in F_5$ such that**

$$F\left[M(Ax, By, t), M(Ax, Ty, t), M(Sy, By, t), M(Ax, Sy, t), M(Sy, Ty, t)\right] \geq 0$$

**Then *A, B, S* and *T* have a unique common fixed point in *X*.**

**Proof: Let $x_0$ be any point in *X*, then by condition (1.1) there exists $x_1, x_2 \in X$ such that $A x_0 = T x_1 = y_0$ and $B x_1 = S x_2 = y_1$.**
**Inductively, we can construct sequences $\{x_n\}$ and $\{y_n\}$ in *X* such that**

$$y_{2n} = Ax_{2n} = Tx_{2n+1},\ y_{2n+1} = Bx_{2n+1} = Sx_{2n+2},\ n = 0, 1, 2, 3.....$$

**Putting** $x = x_{2n},\ y = x_{2n+1}$ *and* $\alpha = (1-q)$ *with* $q \in (0,1)$, *we get*

$$M(Ax_{2n}, Bx_{2n+1}, kt) \geq M(Sx_{2n}, Ax_{2n}, t) * M(Tx_{2n+1}, Bx_{2n+1}, t) * M(Sx_{2n}, Tx_{2n+1}, t) * M(Tx_{2n+1}, Ax_{2n}, (1-q)t) * M(Sx_{2n}, Bx_{2n+1}, (1+q)t).$$

**and so,**

$$M\left(y_{2n}, y_{2n+1}, kt\right) \geq M\left(y_{2n-1}, y_{2n}, t\right) * M\left(y_{2n}, y_{2n+1}, t\right) * M\left(y_{2n-1}, y_{2n}, t\right) * M\left(y_{2n}, y_{2n}, (1-q)t\right) * M\left(y_{2n-1}, y_{2n+1}, (1+q)t\right).$$

$$\geq M\left(y_{2n-1}, y_{2n}, t\right) * M\left(y_{2n}, y_{2n-1}, t\right) * M\left(y_{2n-1}, y_{2n}, t\right) * M\left(y_{2n-1}, y_{2n}, t\right) * M\left(y_{2n}, y_{2n+1}, qt\right).$$

**Since** $t - norm *$ **is continuous, letting** $q \to 1$**, we have**

$$M\left(y_{2n}, y_{2n+1}, kt\right) \geq M\left(y_{2n-1}, y_{2n}, t\right) * M\left(y_{2n}, y_{2n+1}, t\right).$$

**It follows that**

$$M\left(y_{2n}, y_{2n+1}, kt\right) \geq M\left(y_{2n-1}, y_{2n}, t\right) * M\left(y_{2n}, y_{2n+1}, t\right).$$

**Similarly,**

$$M\left(y_{2n+1}, y_{2n+2}, kt\right) \geq M\left(y_{2n}, y_{2n+1}, t\right) * M\left(y_{2n+1}, y_{2n+2}, t\right).$$

**Therefore, for all *n* even or odd, we have**

$$M\left(y_{n}, y_{n+1}, kt\right) \geq M\left(y_{n-1}, y_{n}, t\right) * M\left(y_{n}, y_{n+1}, t\right).$$

**Consequently,**

$$M\left(y_{n}, y_{n+1}, t\right) \geq M\left(y_{n-1}, y_{n}, k^{-1}t\right) * M\left(y_{n}, y_{n+1}, k^{-1}t\right)$$

**By a simple induction, we have**

$$M\left(y_{n}, y_{n+1}, t\right) \geq M\left(y_{n-1}, y_{n}, k^{-1}t\right) * M\left(y_{n}, y_{n+1}, k^{-m}t\right).$$

**Since** $M\left(y_{n}, y_{n+1}, k^{-m}t\right) \to 1 \; as \; m \to \infty$. **It follows that**

$$M\left(y_{n}, y_{n+1}, kt\right) \geq M\left(y_{n-1}, y_{n}, t\right) \; for \; all \; n \in N \; and \; t > 0.$$

**Therefore, by lemma (1),** $\{y_n\}$ **is a Cauchy sequence in *X*.**

**Case (1): Suppose that *S(X)* is a complete subspace of *X*, then the sequence $y_{2n} = Sx_{2n+1}$ is a Cauchy sequence in S(X) and hence has a limit z (say).**

**Now, *z* ∈ *S(X)*, so there exists *w* ∈ *X* such that *z* = *S w*.**

**Since *(A, S)* are semi-compatible, so** $\lim_{n\to\infty} ASx_n = Sz.$

**Step I. Putting** $x = Sx_n$ , $y = x_{n+1}$ *in* $(1.5)$**, we get**

$$F\begin{bmatrix} M\left(ASx_n, Bx_{n+1}, t\right), M\left(ASx_n, Tx_{n+1}, t\right), M\left(Sx_{n+1}, Bx_{n+1}, t\right), \\ M\left(ASx_n, Sx_{n+1}, t\right), M\left(Sx_{n+1}, Tx_{n+1}, t\right) \end{bmatrix} \geq 0.$$

**Letting** $n \to \infty$**, we get**

$$F\left[M\left(Sz, z, t\right), M\left(Sz, z, t\right), M\left(z, z, t\right), M\left(Sz, z, t\right), M\left(z, z, t\right)\right] \geq 0$$

**i.e.,**

$$F\left[M\left(Sz, z, t\right), M\left(Sz, z, t\right), 1, M\left(Sz, z, t\right), 1\right] \geq 0. \textit{ Which implies that } Sz = z.$$

**Step II. Putting** $x = z$, $y = x_{n+1}$ *with* $\alpha = 1$ *in* $(1.2)$**, we get**

$$M\left(Az, Bx_{n+1}, kt\right) \geq M\left(Sz, Az, t\right) * M\left(Tx_{n+1}, Bx_{n+1}, t\right) * M\left(Sz, Tx_{n+1}, t\right) * M\left(Tx_{n+1}, Az, t\right) * M\left(Sz, Bx_{n+1}, t\right).$$

**Taking as** $n \to \infty$,

$$M\left(Az, z, kt\right) \geq M\left(z, Az, t\right) * M\left(z, z, t\right) * M\left(z, z, t\right) * M\left(z, Az, t\right) * M\left(z, z, t\right).$$

**Which implies that** $Az = z = Sz.$

**Step III. As** $A\left(X\right) \subseteq T\left(X\right)$**, there exists some** $u \in X$ **, such that** $z = Az = Tu.$

**Putting** $x = x_{2n}$ , $y = u$ *with* $\alpha = 1$ *in* $(1.2)$**, we have**

$$M\left(Ax_{2n}, Bu, kt\right) \geq M\left(Sx_{2n}, Ax_{2n}, t\right) * M\left(Tu, Bu, t\right) * M\left(Sx_{2n}, Tu, t\right) * M\left(Tu, Ax_{2n}, t\right) * M\left(Sx_{2n}, Bu, t\right).$$

**As** $n \to \infty$, **we get**

$$M(z,Bu,kt) \geq M(z,z,t) * M(z,Bu,t) * M(z,z,t) * M(z,z,t) * M(z,Bu,t).$$

**Which gives** $Bu = z = Tu.$

**But** $(B,T)$ **is weak compatible so** $BTu = TBu$ *i.e.*, $Bz = Tz.$

**Step IV. By putting** $x = z$ , $y = z$ *with* $\alpha = 1$ *in* $(1.2)$ **and assuming that** $Az \neq Bz$ **,**

**We have**

$$M(Az,Bz,kt) \geq M(Sz,Az,t) * M(Tz,Bz,t) * M(Sz,Tz,t) * M(Tz,Az,t) * M(Sz,Bz,t).$$
$$= M(z,z,t) * M(Tz,Tz,t) * M(Az,Bz,t) * M(Bz,Az,t) * M(Az,Bz,t).$$

**Which is a contradiction and gives** $Az = Bz = z.$

**Combining all the results we get** $z = Az = Sz = Bz = Tz.$ **Thus** $z$ **is a common fixed point of A, B, S and T in this case.**

**Case (2): Let** $T(X)$ **be complete.**

**In this case** $z \in T(X)$**. Hence there exists** $w \in X$, *such that* $z = Tw.$

**Step I. Putting** $x = x_{2n}$ , $y = w$ *with* $\alpha = 1$ *in* $(1.2)$**, we get**

$$M(Ax_{2n},Bw,kt) \geq M(Sx_{2n},Ax_{2n},t) * M(Tw,Bw,t) * M(Sx_{2n},Tw,t) * M(Tw,Ax_{2n},t) * M(Sx_{2n},Bw,t)$$

**Letting** $n \to \infty$**, we get**

$$M(z,Bw,kt) \geq M(z,z,t) * M(z,Bw,t) * M(z,z,t) * M(z,z,t) * M(z,Bw,t)$$

*Which implies that* $Bw = z = Tw$**. But (B, T) is weak compatible so** $BTw = TBw.$

**Which further implies that** $Bz = Tz$

**Step II. As (A, S) is semi compatible so** $\lim_n ASx_n \to Sz.$

**By putting** $x = Sx_n$ **,** $y = z$ **(1.5), we get**

**F**$[M(ASx_n, Bz, t), M(ASx_n, Tz, t), M(Sz, Bz, t), M(ASx_n, Sz, t), M(Sz, Bz, t)] \geq 0.$

**That is,**

**F**$[M(Sz, Bz, t), M(Sz, Tz, t), M(Sz, Bz, t), M(Sz, Sz, t), M(Sz, Bz, t)] \geq 0.$

**Which implies that** $Sz = Bz = Tz.$

**Step III. Now, putting** $x = y = z \text{ with } \alpha = 1$ **in (1.2), we get**

$$M(Az, Bz, kt) \geq M(Sz, Az, t) * M(Tz, Bz, t) * M(Sz, Tz, t)$$
$$M(Tz, Az, t) * M(Sz, Bz, t)$$
$$= M(Az, Bz, t) * 1 * 1 * M(Az, Bz, t) * 1$$
$$\geq M(Az, Bz, t).$$

**Thus**

$$Az = Bz = Sz = Tz\,.$$

**Step IV. Again taking** $x = x_{2n}\ ,\ y = z \text{ with } \alpha = 1 \text{ in } (1.2)$**, we get**

$$M(Ax_n, Bz, kt) \geq M(Sx_n, Ax_n, t) * M(Tz, Bz, t) * M(Sx_n, Tz, t) *$$
$$M(Tz, Ax_n, t) * M(Sx_n, Bz, t)$$

**Letting** $n \to \infty$**, we get**

$$M(z, Bz, kt) \geq M(z, z, t) * M(Bz, Bz, t) * M(z, Bz, t) * M(Bz, z, t) * M(z, Bz, t)$$

**Which gives** $z = Bz.$ **Thus** $z = Bz = Az = Sz = Tz.$

**That is z is a common fixed point of A, B, S and T in this case also.**

**Case (3): When** $A(X) \text{ or } B(X)$ **is complete.**

**As** $A(X) \subseteq T(X) \text{ and } B(X) \subseteq S(X)$**, therefore, the result follows from Case (1) and Case (2).**

**Moreover the uniqueness of the fixed point follows from condition (1.2).**

**Example 5: Let *X* = *[0, 1]* equipped with**

$$d(x,y)=|x-y| \text{ and define } M(x,y,t)=\frac{t}{t+d(x,y)} \text{ for all } x,y\in X \text{ and } t>0.$$

**Clearly *(X, M, *)* is a fuzzy metric space with *a * b* = min *{a, b}*.**

**Define self maps *A, B, S, T : X* $\rightarrow$ *X* as**

$$A(x)=\begin{cases} 0, & 0\le x<\frac{1}{2} \\ \frac{1}{2}, & x\ge\frac{1}{2} \end{cases}, \quad B(x)=\begin{cases} x & 0\le x\le\frac{1}{2} \\ 0 & x>\frac{1}{2} \end{cases}$$

$$S(x)=\begin{cases} 0, & x<\frac{1}{2} \\ 1-x & x\ge\frac{1}{2} \end{cases}, \quad T(x)=\begin{cases} x & x<\frac{4}{5} \\ 1 & x\ge\frac{4}{5} \end{cases}$$

**Consider** $\langle x_n\rangle=\frac{1}{2}-\frac{1}{n}$, *then* $Ax_n, Sx_n\rightarrow 0$ *and* $ASx_n=A(0)=S(0)$.

**Thus,** $\lim_n M(ASx_n, S0, t)=\lim_n M(0,0,t)=1$ *for all* $t>0$.

**This implies that *A* and *S* are semi-compatible.**

**Now,**

$$Bx=Tx \text{ for all } x\in\left[0,\frac{1}{2}\right] \text{ and } BTx=Bx=x=Tx=TBx \text{ for all } x\in\left[0,\frac{1}{2}\right].$$

**Which implies that *B* and *T* are weak compatible. Also, *A, B, S* and *T* are all discontinuous.**

**Moreover,**

$$A(X)\subseteq T(X) \text{ and } B(X)\subseteq S(X).$$

**Here, *A, B, S* and *T* satisfy all the conditions of our theorem with *k* $\in$ *(0, 1)* and *A, B, S* and *T* have a unique common fixed point *x* = 1/2.**

**If we take *A* = *B* = *f* and *S* = *T* = *g* in theorem 1, we get the following corollary:**

**Corollary 1: Let *(X, M, *)* be a fuzzy metric space with $a * a \geq a$ for all $a \in [0, 1]$ and with condition (FM-6) and let *A, B, S, T* : $X \to X$ be self maps satisfying (1.1) , (1.2), (1.4), (1.5) and the pairs *(A, S)* and *(B, T)* are semi-compatible. Then *A, B, S* and *T* have a unique common fixed point in *X*.**

**Proof: As semi-compatibility implies weak compatibility, the proof follows from theorem 1.**

**On taking $A = B$ in theorem 1, we have the following corollary.**

**Corollary 2: Let *(X, M, *)* be a fuzzy metric space with $a * a \geq a$, $a \in [0, 1]$ and *A, S* and $T : X \to X$ satisfying (1.4)**

**(i)** $A(X) \subseteq T(X) \cap S(X)$

**(ii)The pair *(A , S)* is semi compatible and *(A , T)* is weak compatible**

**(iii) There exists $k \in (0, 1)$ such that**

$$M(Ax, Ay, kt) \geq M(Sx, Ax, t) * M(Ty, Ay, t) * M(Sx, Ty, y) * M(Ty, Ax, \alpha t) * M(Sx, Ay, (2-\alpha)t)$$
$$for\ all\ x, y \in X\ ,\ \alpha \in (0,2)\ and\ t > 0.$$

**(iv) There exists $F \in F_5$ such that**

$$F\begin{bmatrix} M(Ax, Ay, t), M(Ax, Ty, t), M(SY, Ay, t) \\ M(Ax, Sy, t), M(Sy, Ty, t) \end{bmatrix} \geq 0.$$

**Then *A, S* and *T* have a unique common fixed point in *X*.**

**Now, taking $S = I$ and $T = I$ in theorem 1, we get the following corollary.**

**Corollary 3: Let *(X, M, *)* be a fuzzy metric space with $a * a \geq a$ for all $a \in [0, 1]$ and with condition (FM-6) and let *A, B*: $X \to X$ be self maps satisfying (1.1), (1.4) and**

**(iii) There exists $k \in (0, 1)$ such that**

$$M(Ax,By,kt) \geq M(x,Ax,t) * M(y,By,t) * M(x,y,t) * M(y,Ax,\alpha t) * M(x,By,(2-\alpha)t)$$

*for all* $x, y \in X$ , $\alpha \in (0,2)$ *and* $t > 0.$

**(iv) There exists $F \in F_5$ such that**

$$F\begin{bmatrix} M(Ax,By,t), M(Ax,y,t), M(Y,By,t) \\ M(x,Ay,t), M(x,Bx,t) \end{bmatrix} \geq 0.$$

**Then *A* and *B* have a unique common fixed point in *X*.**

## REFERENCES


1. B. Singh and S. Jain, Int. J. Math. Math. Sci., 16 (2005) 2617.
2. B. Singh and S. Jain, J. Chungcheong Math. Sci., 17(1) (2004) 1.
3. B. Singh and S. Jain, J. Chungcheong Math. Sci., 18(1) (2005) 1.
4. B. Singh and S. Jain, Int. J. Math. Math. Sci., 5 (2005) 789.
5. U. Mishra, A. S. Ranadive and D. Gopal, Tamkang J. Maths., 39(4) (2008) 309.
6. Y. J. Cho, H. K. Pathak, S. M. Kang, J. S. Jung, Fuzzy Sets & Syst., 93 (1998) 99.
7. L. M. Saliga, Int. J. Math. Math. Sci., 19(1) (1996) 103.
8. B. K. Sharma, D. R. Sahu, M. Bounias and A. Bonaly, Int. J. Math. Math. Sci., 21(2) (1995) 277.
9. V. Popa, Bul. Stiint. Univ. Baia Mare Ser. B. Fasc. Mat. Inform. 18(1) (2002) 105.
10. D. Turkohlu and I. Altun, Bull. Del. La Soc. Math. Mexicana, 13(1) (2007) 195.
11. I. Altun and D. Turkoglu, Filomat, 22(1) (2008) 11.
12. S. Kutukcu, S. Sharma and H. Tokgoz, Int. J. Math. Anal., 1(18) (2007) 861.
13. R. P. Pant, J. Math. Anal. Appl., 226 (1998), 251.

PK ISSN 0022- 2941; CODEN JNSMAC
Vol. 49, No.1 & 2 (April & October 2009) PP 49-57

# PREPARATION AND CHARACTERIZATION OF $SrBi_2Ta_2O_9$ (SBT) THIN FILMS

**Z. N. KAYANI, S. RIAZ AND S. NASEEM**

Centre for Solid State Physics, University of the Punjab, Lahore-54590, Pakistan
*E-mail Addresses: zohrakayani@yahoo.com

(Received: August 10, 2011)

**ABSTRACT:** Steady sol and gel of $SrBi_2Ta_2O_9$ (SBT) was prepared using penta-ethoxy tantalum, strontium acetate, and bismuth nitrate as raw materials, acetic acid and ethanol as solvents. SBT thin films with 200 nm thickness were prepared on copper substrates using the spin coating method. In this work the approach to improve the synthesis of SBT thin films by a sol–gel procedure is studied and their effects on the thin film properties are evaluated. XRD and scanning electron microscopy (SEM) analysis was obtained. X-ray diffraction (XRD) studies have been carried out to assess the crystallinity and phase formation. The surface features of the films, studied by scanning electron microscopy and optical microscopy reveal the grain growth pattern. Electrical characterisation of the films such as I–V measurements have been carried out.

**Keywords:** Ferroelectric thin films, SBT thin films, Sol–gel technique, Optical and electrical characterisation.

## 1. INTRODUCTION

Ferroelectric bismuth-layered compounds were first studied by Aurivillius and Fang [1]. These structures consist of alternate bismuth oxide and perovskite type layers. Bi-layer structured compounds are generally represented by the following formula:

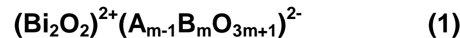

$$(Bi_2O_2)^{2+}(A_{m-1}B_mO_{3m+1})^{2-} \qquad (1)$$

where A is $Bi^{3+}$, $Ba^{2+}$, $Sr^{2+}$, $Ca^{2+}$, $Pb^{2+}$, $K^+$ or $Na^+$ and B is $Ti^{4+}$, $Nb^{5+}$, $Ta^{5+}$, $Mo^{6+}$, $W^{6+}$ or $Fe^{3+}$, and *m* is a whole number from 1 to 8 or a fraction such as 2(1/2) or 3(1/2). A is the cation of coordination 12 in the perovskite sublattice and B is the octahedral site. Bi forms the oxide interlayer $(Bi_2O_2)^{2+}$ between the perovskite blocks $(A_{m-1}B_mO_{3m+1})^{2-}$, where *m* is the number of octahedral layers inside the perovskite sublattice of the

**structure. For the stoichiometric composition $SrBi_2Ta_2O_9$ (SBT), m = 2; thus, there is a complete perovskite sublattice created by the Ta-O octahedra in which a cation A of coordination 12 (*i.e.*, Sr) can reside. [2]**

**Ferroelectric layered perovskites of the Aurivillius family are used as non-volatile Ferroelectric Random Access Memory (FRAM) devices in smart card technology. Paz de Araujo et al. [3] described a layered superlattice material that was suitable for forming a low fatigue ferrorelectric. Applications of this material are in memory devices, specifically non-volatile and volatile memories. Some specific layered-perovskite materials that are disclosed for use in this application are strontium bismuth tantalate ($SrBi_2Ta_2O_9$), strontium bismuth tantalum niobate ($SrBi_2TaNbO_9$), bismuth titanate ($Bi_4Ti_3O_{12}$), lead bismuth tantalate ($PbBi_2Ta_2O_9$), and barium bismuth niobate ($BaBi_2Nb_2O_9$). Layered superlattice materials are defined by Paz de Araujo et al. as having a localized structure, within a grain or a larger or smaller unit, wherein the localized structure contains predominately repeatable units containing one or more perovskite-like layers and one or more intermediate non-perovskite-like layers that are spontaneously linked in an interdependent manner.**

**$SrBi_2Ta_2O_9$ is well studied bismuth layered perovskites with applications in Non-Volatile Ferroelectrics Random Access Memories (NVFRAMs), due to their high fatigue endurance ($10^{12}$ cycles) under polarization switching. The modern computer industry requires dimensions of NVFRAMs should be as small as possible and so SBT to be used as thin films [3].**

**Thin film of $SrBi_2Ta_2O_9$ can be prepared by pulsed laser deposition [4], metal organic chemical vapor deposition [5], metal organic decomposition [6] and the sol-gel method [7]. As the sol-gel process can be used to produce large-area films at temperatures <700°C, there has been interest in using the sol-gel process to prepare ferroelectric thin films [8]. However, as starting materials, alkoxides would make the whole fabricating process more susceptible to temperature and ambient humidity, and must be handled under inert atmosphere. Therefore, the alkoxides of some metals**

**such as Ta and Bi were coordinated using pyridine [9], alcohol–amine [10] and acetylacetone [11], and metal complex compound became stable. But the addition of complex agent makes it difficult for the control of the processes of gel polymerization. In order to overcome these problems, new solvent are used, thus stable SBT precursor solution can be prepared to allow their handling in air, which makes the operation more convenient. In this paper, the synthesis of SBT films by a sol-gel process and the measurements of the properties of these thin films will be reported.**

## 2. EXPERIMENTAL PROCEDURES

**Preparation of thin films: The starting materials used were: strontium acetate ($Sr(CHCOO)_3$. 1/2 $H_2O$); bismuth nitrate ($Bi(NO_3)_3.5H_2O$), tantalum ethoxide ($Ta(CH_3CH_2O)_5$ and glacial acetic acid as the solvent. Bismuth nitrate rather than alkoxide of bismuth was used as bismuth source to prepare stable SBT sol. Thus, the hydrolysis and polymerization reaction is easier to control. The new approach described here for preparing SBT thin films starts with the solubilization of bismuth nitrate and strontium acetate hemihydrate in a minimum quantity of acetic acid. The obtained solution was diluted in ethanol. The last step was the addition of tantalum ethoxide. The sol was refluxed at 60°C for five hours. The solution was then cooled to room temperature under stirring, thereby giving a Sr-Bi-Ta complex transparent solution. Synthesis route of $SrBi_2Ta_2O_9$ is given in Fig. 1.**

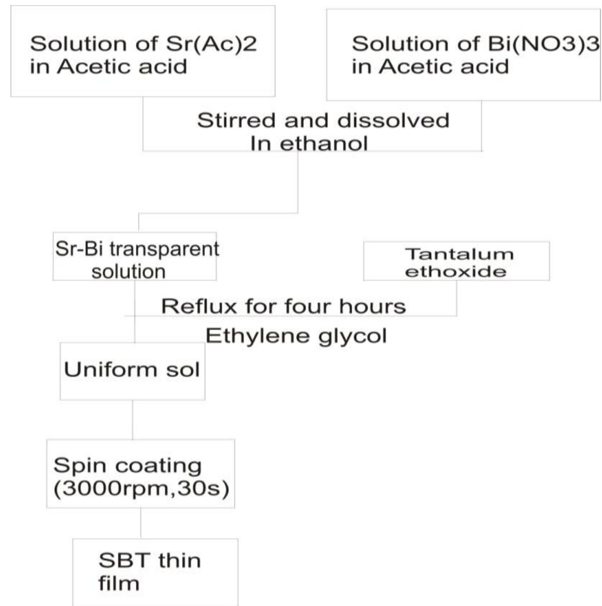


**Fig. 1: Scheme for the preparation of $SrBi_2Ta_2O_9$ thin film by using cobalt chloride and ammonia**

**In the present study, copper substrate was used for the deposition of SBT thin films. The substrate was ultrasonically cleaned in acetone, followed by iso-propanol. Film was prepared by spin coating the cooled solution at 3000 rpm for 30 s. To prepare thicker film, the spin coating process was repeated. After spin coating the substrate, the film was kept in ambient air for 1 h to form gel films by hydrolysis and polymerization. Heat treatment of dried film was carried out at a temperature of 300°C for 2 hrs. The Crystallization, densification and microstructure of the films were examined.**

## 3. RESULTS AND DISCUSSION

### 3.1 X-RAY DIFFRACTION (XRD) STUDIES

**Figure 2 shows the X-ray diffraction patterns of the $SrBi_2Ta_2O_9$ thin films of as-deposited film, heated film at 300 °C for one hour and then for two hours at same temperature.**

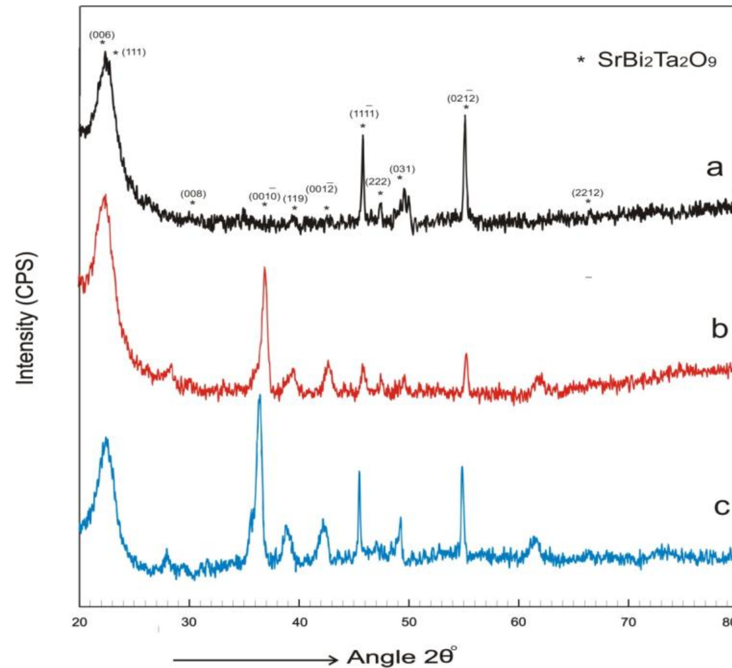


**Fig. 2: XRD patterns of the $SrBi_2Ta_2O_9$ thin film (a) as deposited, (b) heated for one hour at 300°C, (c) heated for two hours at 300°C.**

**In Fig. 2a shows the XRD pattern for the $SrBi_2Ta_2O_9$ thin film deposited on copper substrate. Peaks of copper are omitted intentially. Three diffraction peaks were of $SrBi_2Ta_2O_9$.**

**In Figs. 2b and 2c exhibit the XRD patterns for annealed $SrBi_2Ta_2O_9$ thin films at 300 °C temperature for 1 hour and for two hours respectively. Figure 3.9 shows that intensity of the SBT diffraction peak at $2\theta$ = 34.844° became strong at one and two hours heating. There were no diffraction peaks at $2\theta$ = 39.420° and 42.662° for the as-deposited film that appeared at one hour heating and intensified at two hours heating. Diffraction peaks at $2\theta$ = 45.645°, 47.233° 49.233° and 54.976° became less intense on one hour heating but their intensity increased with prolonged heating. Evaluating Williamson-Hall relation [12] Figs. 3(a) and 3(b) show variation in grain size and strain with increase in time of heating. The average grain sizes for the $SrBi_2Ta_2O_9$ is in the range of 15.404–38.51 nm, shown in Fig. 3(a) which**

**indicates that the grain size of the $SrBi_2Ta_2O_9$ film increased as the annealing temperature increased. Grain size of the as-deposited $SrBi_2Ta_2O_9$ was 15.404 nm. It was 38.51 nm after heating the film at 300°C for 60 minutes but prolonged heating at same temperature again decreased the grain size to 25.63 nm. This effect may have been the cause of rearrangement of the grains in these films during heating and the sample temperature is not too high for the final attainment of grain size and structure.**

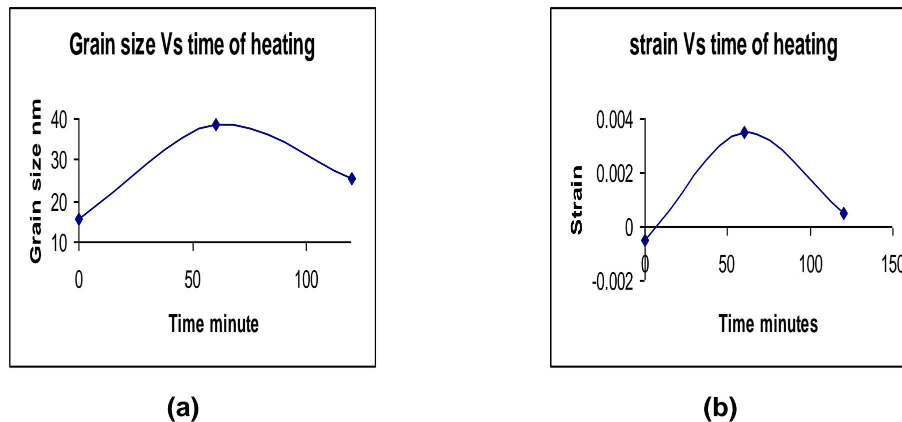


**(a) (b)**

**Fig. 3: Dependence of grain size (a) and strain (b) on time of heating evaluated by Williamson-Hall relation [6]**

## 3.2 SCANNING ELECTRON MICROGRAPHS (SEM) STUDIES

**SEM images of an SBT thin film are shown in Figure 4. These micrographs indicate that the surface is homogeneous, grains are very dense and no secondary structures can be seen between the grains. Same surface analysis of SBT thin film is reported by other researchers [13,14,15]. Dense but more elongated grains are reported by Aguilar [16,17].**

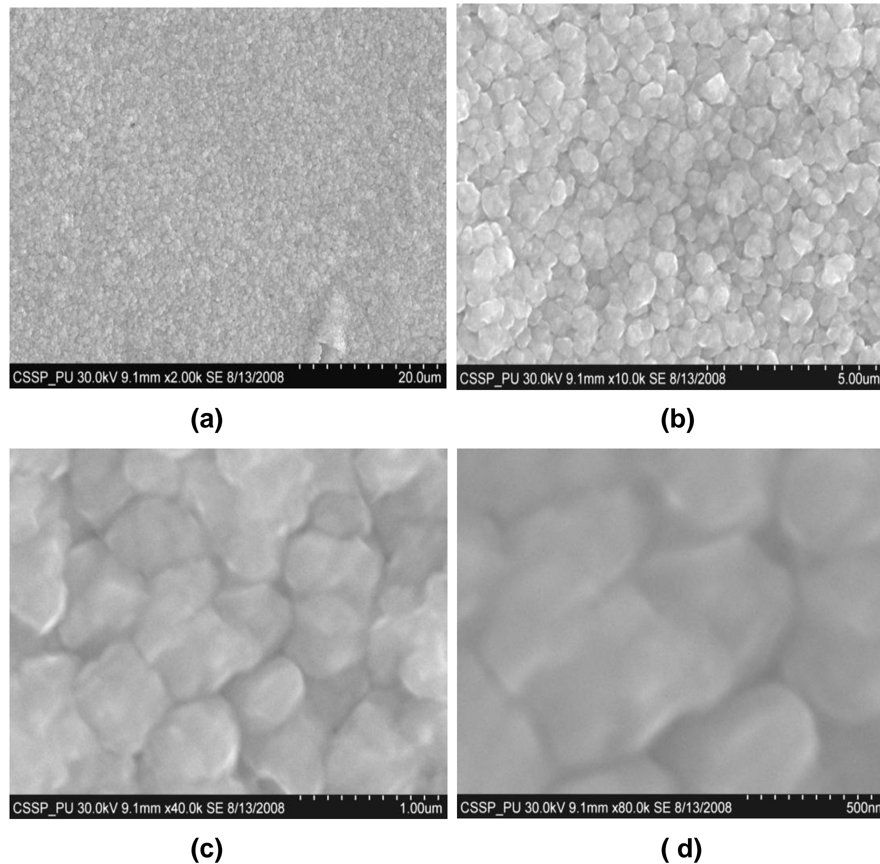


**Fig. 4: Scanning electron micrographs of thin film of $SrBiTa_3O_9$ with (*a*) magnification of 2000x, (b) magnification of 10000x, (c) magnification of 40000x and (d) magnification of 80000x**

**3.3 ELECRICAL PROPERTIES**

**Figure 5 shows I-V characteristics of SBT thin film. I-V measurements of SBT thin film heated for two hours at 300 °C showed ohmic behaviour with negligible current (in nano-ampere range). The resistivity that was calculated from this plot is of the order of 1.7 MΩ-cm, which is as expected from such films.**

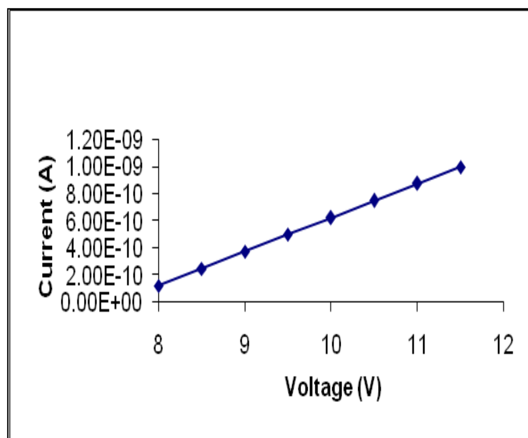


**Fig. 5: I-V characteristics of SBT thin film.**

## 4. CONCLUSIONS

**SBT films were successfully synthesised by using sol-gel technology. Steady sol of $SrBi_2Ta_2O_9$ (SBT) was prepared by using strontium acetate ($Sr(CHCOO)_3$. 1/2 $H_2O$); bismuth nitrate ($Bi(NO_3)_3.5H_2O$), tantalum ethoxide ($Ta(CH_3CH_2O)_5$), and glacial acetic acid as the solvent. XRD confirmed formation of SBT compound. The Scanning electron micrographs indicated that the surface was homogeneous, grains were dense and no secondary structures could be seen between the grains. Same surface analysis of SBT thin film was reported by other researchers [13,14,15]. Dense but more elongated grains were reported by Aguilar [16,17].**

## REFERENCES

1. **B. Aurivillius and P. H. Fang, Phys. Rev., 126 (1962) 893.**
2. **M. A. Rodriguez, T. J. Boyle, B. A. Hernandez, C. D. Buchheit and M. O. Eatough, J. Mater. Res., 11 (1996) 2282.**
3. **C. A. Paz de Araujo, J. D. Cuchiaro, M. C. Scott and L. D. Mcmillan, International Patent Applicant, International Publication No. WO 93/12542, (1993).**
4. **H. Tabata, H. Tanaka and T. Kawai, Jpn. J. Appl. Phys., 34 (1995) 5146.**

5. T. Li, Y. Zhu, S. B. Desu, C. H. Peng and M. Nagata, Appl. Phys. Lett., 68 (1996) 616.
6. K. Amanuma, T. Hase and Y. Miyasaka, Appl. Phys. Lett., 66 (1995) 221.
7. T. Atsuki, N. Soyama, T. Yonezawa and K. Ogi, Jpn. J. Appl. Phys., 34 (1995) 5096.
8. J. D. Mackenzie, J. Non-Cryst. Solids, 100 (1988) 162.
9. T. J. Boyle, C. D. Buchheit, M. A. Rodriguez, H. N. Shareef, B. A. Hernandez, B. Scott and J. W. Ziller, J. Mater. Res., 11 (1996) 2274.
10. W. Wang, Y. Zhou, S. Chen, F. Ye and D. C. Jia, J. Mater. Sci. Technol., 17 (2001) 25.
11. T. Hayashi, H. Takahashi and T. Hara, Jpn. J. Appl. Phys., 35 (1996) 4952.
12. H. P. Klug and L. E. Alexander, *X-ray Diffraction procedures for polycrystalline and amorphous materials,* Wiley, New York, 1974.
13. T. Y. Lim, K. H. Yang, B. H. Kim and K. H. Auh, Thin Solid Films, 471 (2005) 12.
14. Q. F. Zhou, H. L. W. Chan and C. L. Choy, J. Non-Cryst. Solids, 254 (1999) 106.
15. Y. Kim, H. K. Chae, K. S. Lee and W. I. Lee, J. Mater. Chem., 8 (1998) 2317.
16. G. G. Aguilar, I. M. Salvado and M. E. Costa, Mat. Lett, 60 (2006) 28.
17. G. G. Aguilar, M. E. V. Costa and I. M. Salvado, J. Eur. Cer. Soc., 25 (2005) 2331.